Acta Pharmacologica Sinica

www.nature.com/aps

ARTICLE

Activating Wnt/β-catenin signaling by autophagic degradation of APC contributes to the osteoblast differentiation effect of soy isoflavone on osteoporotic mesenchymal stem cells

Jing Ge[1], Ye-jia Yu[1], Jia-yi Li[1], Meng-yu Li[1], Si-mo Xia[1], Ke Xue[2], Shao-yi Wang[1]✉ and Chi Yang[1]✉

The functional role of autophagy in regulating differentiation of bone marrow mesenchymal stem cells (MSCs) has been studied extensively, but the underlying mechanism remains largely unknown. The Wnt/β-catenin signaling pathway plays a pivotal role in the initiation of osteoblast differentiation of mesenchymal progenitor cells, and the stability of core protein β-catenin is tightly controlled by the APC/Axin/GSK-3β/Ck1α complex. Here we showed that genistein, a predominant soy isoflavone, stimulated osteoblast differentiation of MSCs in vivo and in vitro. Female rats were subjected to bilateral ovariectomy (OVX); four weeks after surgery the rats were orally administered genistein (50 $mg{\cdot}kg^{-1}{\cdot}d^{-1}$) for 8 weeks. The results showed that genistein administration significantly suppressed the bone loss and bone-fat imbalance, and stimulated bone formation in OVX rats. In vitro, genistein (10 nM) markedly activated autophagy and Wnt/β-catenin signaling pathway, and stimulated osteoblast differentiation in OVX-MSCs. Furthermore, we found that genistein promoted autophagic degradation of adenomatous polyposis coli (APC), thus initiated β-catenin-driven osteoblast differentiation. Notably, genistein activated autophagy through transcription factor EB (TFEB) rather than mammalian target of rapamycin (mTOR). These findings unveil the mechanism of how autophagy regulates osteogenesis in OVX-MSCs, which expands our understanding that such interplay could be employed as a useful therapeutic strategy for treating postmenopausal osteoporosis.

Keywords: autophagy; wnt/β-catenin signaling pathway; osteoporosis; bone marrow mesenchymal stem cells

Acta Pharmacologica Sinica (2023) 44:1841–1855; https://doi.org/10.1038/s41401-023-01066-x

INTRODUCTION

Postmenopausal osteoporosis (PMOP) is a common skeletal metabolic disorder which compromises bone strength and the healing process. It is characterized by gradually reduced bone mineral density and deterioration of the bone microarchitecture. Autophagy, a major catabolic pathway responsible for the elimination of damaged proteins and organelles, has been proved to be critical in maintaining bone homeostasis [1–3]. Increasing evidence has uncovered the relationship between autophagy and osteoporosis, providing an exciting opportunity to target autophagy for the prevention and treatment of osteoporosis [4]. Under estrogen deprivation, the endogenous bone marrow mesenchymal stem cells (MSCs) exhibit impaired autophagy activity and reduced osteogenic differentiation capability [5]. Treatment with autophagy inducer rapamycin promoted osteoblastic differentiation of MSCs derived from ovariectomized (OVX) mice in vitro and mitigated the OVX-induced osteoporotic phenotype in vivo [5]. However, the exact mechanism of how autophagy regulates OVX-MSCs differentiation remains to be elucidated.

Genistein, a predominant soy isoflavone, has been reported to possess anti-resorptive and bone-sparing effects in postmenopausal women [6, 7] and OVX-animals [8, 9]. Various studies have reported that genistein is able to stimulate osteogenic differentiation of MSCs in vitro [10–13]. However, all these studies conducted experiments by using MSCs from healthy rodents, which are distinct from OVX-MSCs. Interestingly, genistein is found to have an autophagy activating effect in neurons [14] and tumor cells [15], but its effect on modulating the autophagy process in MSCs has not been reported so far. Therefore, two major issues need to be resolved. First, as previous studies used MSCs from healthy animals for the in vitro experiments, the effect of genistein on OVX-MSCs is still unknown. Second, the mechanism of genistein on differentiation of OVX-MSCs is currently unclear.

The canonical Wnt signaling pathway plays a pivotal role in the initiation of osteoblast differentiation of mesenchymal progenitor cells [16]. Beta-catenin, the main effector of canonical Wnt signaling pathway, is regulated by the β-catenin destruction complex. In the β-catenin destruction complex, adenomatous polyposis coli (APC) protein and Axin collaborate to co-recruit the kinases casein kinase 1 (CK1) and glycogen synthase kinase 3β (GSK3β) jointly with their substrate β-catenin. This enables the sequential phosphorylation of β-catenin, and triggers proteasomal

[1]Department of Oral Surgery, Shanghai Ninth People's Hospital, Shanghai Jiao Tong University School of Medicine; College of Stomatology, Shanghai Jiao Tong University; National Center for Stomatology; National Clinical Research Center for Oral Diseases; Shanghai Key Laboratory of Stomatology; Shanghai Research Institute of Stomatology, Shanghai 200001, China and [2]Department of Pastic and Reconstructive Surgery, Shanghai Ninth People's Hospital, Shanghai Jiao Tong University School of Medicine, Shanghai 200001, China
Correspondence: Shao-yi Wang (598092050@qq.com) or Chi Yang (yangchi63@hotmail.com)

Received: 29 October 2022 Accepted: 17 February 2023
Published online: 27 March 2023

degradation of β-catenin eventually [17]. While the regulation of β-catenin by APC has been extensively studied, the regulation of APC itself has received little attention.

In the present study, we found that genistein inhibited bone loss, downregulated P62 levels and rebalanced the dysregulated osteoblast-adipocyte differentiation of MSCs in the femurs and tibias of OVX rats. In vitro, genistein-induced autophagy activated Wnt/β-catenin signaling pathway by promoting APC degradation, resulting in osteoblastic differentiation of OVX-MSCs. In addition, we demonstrated that autophagy activation by genistein was delivered by transcription factor EB (TFEB) upregulation and nuclear translocation rather than the mTOR pathway.

MATERIALS AND METHODS

Reagents, antibodies, plasmids, and RNA interference

Genistein and cycloheximide were purchased from Sigma (Sigma-Aldrich Inc., St. Louis, MO, USA). Bafilomycin A1 (Baf-A1) and MG132 were obtained from CST (Cell Signaling Technology, Beverly, MA, USA). Antibodies were from various sources, including Abcam (anti-LC3b, anti-P62, anti-APC, anti-Runx2, anti-Bmp2, anti-Axin2, anti-Fabp4 and anti-rabbit IgG), CST (anti-P62, anti-LC3b, anti-β-catenin, anti-active-β-catenin, anti-Dvl2, anti-GSK-3β, anti-p-GSK-3β, anti-Atg7, anti-Ulk1, anti-mTOR, anti-p-mTOR, anti-p-p70S6K [Thr389], anti-Histone H3, anti-β-actin, HRP-conjugated anti-rabbit and HRP-conjugated anti-mouse), Santa Cruz Biotechnology (anti-CK1α and anti-APC), Invitrogen (anti-osteocalcin, anti-TFEB and anti-LepR).

Atg7 siRNAs, Ulk1 siRNAs, Ctnnb1 siRNAs, TFEB siRNAs, Control siRNAs and mRFP-GFP tandem fluorescently tagged LC3 adeno-viral vector were purchased from HanBio Technology (Shanghai, China). The sequences of rat siRNA are as follows:

Atg7: 5′-GCAUCAUCUUUGAAGUGAA-3′;
Ulk1: 5′-GCAUUGGCACCAUUGUCUA-3′;
Ctnnb1: 5′-CCACUAAUGUCCAGCGCUU-3′;
TFEB: 5′-GCGAGAGCUAACAGAUGCU-3′;
Scrambled siRNA: 5′-UUCUCCGAACGUGUCACGU-3′;

Experimental animals

All experiments were performed with the approval of the Ethics Committee of Shanghai Jiao Tong University School of Medicine. This study conformed to the Guidelines for the Care and Use of Laboratory Animals published by the US National Institutes of Health (NIH publication No. 85-23, revised 1985).

Sixty 3-month-old female Sprague-Dawley rats, mean weight 221 ± 23 g, were obtained from the Ninth People's Hospital Animal Center (Shanghai, China). Rats were maintained under controlled conditions of room temperature (25 °C), relative humidity (50%–80%) and illumination (12 h light, 12 h dark). All rats had free access to a diet low in phytoestrogen content and water.

Following 2 week of adaptation, 60 rats were randomly divided into 2 groups: (1) Sham group, rats received the operation while ovaries were not removed (Sham, $n = 30$), (2) bilateral ovariectomy (OVX, $n = 30$). After 4-week of endogenous hormonal decline, the rats in both groups were randomly divided into 2 sub-groups ($n = 15$/group), and either treated with genistein (50 mg/kg body weight) (Sham+GEN and OVX + GEN) or PBS vehicle (Sham+VEH and OVX + VEH) by gastric gavage once daily. Eight weeks after genistein/PBS administration, blood was collected before rats were sacrificed by cervical dislocation under halothane anesthesia. Bilateral femurs and tibias were dissected out and fixed in 10% neutral-buffered formalin for further analysis.

A double fluorescent labeling method was carried out on rats for the histomorphometric analysis according to previous description [18]. All rats were injected (i.p.) with alizarin red s (30 mg/kg, AL, Sigma) and calcein (20 mg/kg, CA, Sigma) at 5-week and 1 week before necropsy, respectively.

Serum biochemistry

Serum samples were collected and stored immediately at −80 °C for analysis. Serum was measured in duplicate by commercially available ELISA kits for the following: bone-specific alkaline phosphatase (b-ALP; CUSABIO, Wuhan, China) and type 1 collagen C-terminal telopeptide (CTX-1; Elabscience Biotechnology, Wuhan, China).

Micro-CT analysis

The distal femurs were scanned using a micro-CT scanner (skyscan1176, Bruker, Belgium) at 90 kV/278 mA, with resolution of 18 μm. To analyze trabecular bone, a region of 2.5 mm of the distal metaphysis starting 0.4 mm from the proximal end of the distal femoral growth plate was identified as region of interest (ROI). The 3D reconstructions of ROI were analyzed using the evaluation software of the micro-CT system. The following parameters were measured: bone mineral density (BMD), bone volume fraction (BV/TV), trabecular thickness (Tb. Th.) and spacing (Tb. Sp.) were calculated after applying a constant threshold.

Bone histomorphometric study

Bone histomorphometric study was carried out as described previously [19]. Briefly, proximal tibias were fixed, dehydrated and embedded in methyl methacrylate resin. Longitudinal sections were cut, ground and polished to a final thickness of 80 μm. Region of interest was located in the trabecular bone which was 0.4 mm away from the growth plate. Mineral appositional rate (MAR) and bone-formation rate (BFR/BS) were measured using Osteomeasure system (Osteometrics, Inc., Atlanta, GA, USA) to reflect the growth of new bone.

Histology, immunohistochemistry and immunofluorescence staining

Decalcification of specimens was carried out with 10% EDTA with constant shaking for 2 months. After decalcification, the specimens were embedded in paraffin and cut into 5 μm-thick sections.

For haematoxylin and eosin (H&E) staining, three sections of the most central part of the distal femur were selected, stained with H&E and examined under a light microscope for the observation.

For the osteocalcin (Ocn) and fatty acid binding protein 4 (Fabp4) immunohistochemistry, sections were deparaffinized and rehydrated. After antigen retrieval and background blocking, the sections were then incubated with anti-Ocn antibody (1:200) or anti-Fabp4 antibody (1:50) at 4 °C overnight. The sections were then washed in PBS and incubated with secondary antibody, and stained with DAB kit. Digital images of the sections were captured by a light microscope (Olympus BX50, Olympus Corp, Japan). For quantification of Ocn and Fabp4 staining, number of osteoblasts per adjacent bone surface (*n*/mm) and area of adipocytes per square millimeter of bone marrow area (%) were calculated with Image-Pro Plus V6.0.0, respectively.

For P62 and leptin receptor (LepR) immunofluorescence staining, sections were blocked with 10% goat serum (Gibco) and then incubated with primary antibodies (anti-P62, 1:50, Abcam; anti-LepR, 1:50, Invitrogen) at 4 °C overnight and with a secondary antibody for 1 h at 37 °C. Slides were then stained with DAPI and mounted with an anti-fade reagent (Invitrogen). The images were captured by a Zeiss LSM710 confocal microscope (Carl Zeiss).

Cell culture, genistein treatment and autophagy inhibition treatment

Twelve-week-old female Sprague-Dawley rats were performed bilateral ovariectomy via the dorsal approach. Twelve weeks after surgery, OVX-MSCs were harvested from the bone marrow of the tibias and femurs of OVX rats. Healthy-MSCs were harvested from the bone marrow of the tibias and femurs of 6-month-old female Sprague-Dawley rats. The protocol of isolation and culture of MSCs

was adopted from previous study [20]. OVX-MSCs were cultured in DMEM medium without phenol red (Gibco, Grand Island, NY, USA) supplemented with 10% FBS (Gibco) and 100 U/mL penicillin/streptomycin (Invitrogen, Carlsbad, CA, USA) at 37 °C under the condition of a 5% CO_2 humidified atmosphere, and the medium was replaced every 3 days. Healthy-MSCs were cultured in the same condition except that the DMEM medium contained phenol red (Gibco). Cells at passage 2 were used in this study. C3H10T1/2 cells (purchased from Cell Bank of the Chinese Academy of Sciences) were cultured in α-MEM supplemented with 10% FBS (Gibco) and 100 U/mL penicillin/streptomycin (Invitrogen, Carlsbad, CA, USA).

To evaluate the effect of genistein on osteogenic differentiation and autophagy, genistein was added to the media at a range of dosages (0, 1, 10, 100, 1000 nM). Cycloheximide and MG132 were used at 5 μg/mL and 5 μM, respectively. Bafilomycin A1 (Baf-A1) was applied at 10 nM. To induce osteoblast differentiation, osteogenic medium (OM) was made by complete medium supplemented with 50 μM ascorbic acid, 10 mM sodium β-glycerophosphate and 10 nM dexamethasone (Sigma).

Phenotypic characterization

For the phenotypic characterization, cells of P2 were stained with FITC-conjugated antibodies for 30 min at 4 °C followed by extensive washing with PBS. The following antibodies were used at 5 μl per million cells: CD44 (Elabscience, E-AB-F1225C), CD90 (Elabscience, E-AB-F1226C), CD45 (Elabscience, E-AB-F1227C), CD31 (Abcam, ab33858), IgG2a (Elabscience, E-AB-F09802C) and IgG1 (Elabscience, E-AB-F09792C) isotype control of IgG. All samples were resuspended in 500 μL PBS and analyzed by flow cytometer (Beckman, CytoFLEX LX).

Knockdown of Atg7, Ulk1, Ctnnb1, and TFEB by RNA interference siRNA

SiRNA transfection was conducted according to the manufacturer's protocol. Briefly, one day before transfection, cells were seeded in 6-well plate that they will be 50%–60% confluent at the time of transfection. siRNA 200 pmol was diluted in 200 μL Opti-MEM reduced serum medium (Gibco), mixed gently and 8 μL RNAfit was added (HanBio Technology). The sample was mixed gently and incubated for 10 min at room temperature. The siRNA-RNAfit complexes were added to each well, mixed gently and the cells were incubated for 48 h at 37 °C in a CO_2 incubator. Quantitative real-time PCR (qRT-PCR) and Western blotting were used to determine the efficacy of siRNA interference.

Cell counting kit-8 (CCK-8) assay

The MSCs were seeded at 3×10^3 cells/well onto 96-well plates and cultured overnight, and the culture medium was replaced with various concentrations of genistein for 7 days. The cell viability was assessed using the cell counting kit-8 (Dojindo, Kumamoto, Japan). A total of 10 μL of CCK-8 solution was added to each well and then incubated for 2 h at 37 °C. The optical density (*OD*) at 450 nm was measured by microplate reader (ELx800; BioTek Instruments, USA).

Alkaline phosphatase (ALP) staining/activity and Alizarin Red staining and quantification

Cells were fixed and stained using ALP staining kit (Beyotime Biotechnology, Shanghai, China). ALP quantitative assay was performed according to previous study [21]. Briefly, cells were lysed, and protein lysates were incubated with substrate p-nitrophenyl phosphate (pNPP) (Sigma) at 37 °C for 30 min. ALP activity was measured by testing *OD* values at 405 nm. The total protein content of the cells was measured by BCA protein assay kit (Beyotime). ALP activity was expressed as the *OD* values per milligram of total proteins. The relative fold change in ALP activity was shown.

After culturing in OM for 14 days, cells were stained by alizarin red (Sigma) at room temperature for 10 min then rinsed by PBS. For the quantitative analysis of Alizarin Red, the stained cultures were destained with acetylpyridinium chloride (100 mM; Sigma) for 1 h at room temperature. The absorbance of the released stain was measured at 562 nm with microplate reader (ELx800; BioTek Instruments, USA).

Oil-Red-O staining and measurement

Adipogenic induction was performed by commercial kits (Cyagen, China) according to the manufacturer's instructions. After 2 weeks' induction, cell monolayers were fixed in 4% formaldehyde, washed in PBS and stained with a 0.6% (*w/v*) Oil-Red-O solution (60% isopropanol, 40% water) for 15 min at room temperature.

Transmission electron microscopy (TEM) analysis

OVX-MSCs were digested and washed twice with PBS and primarily fixed in 2.5% glutaraldehyde overnight. The samples were post-fixed in 1% osmium tetroxide for 1 h. After washing with PBS, the samples were progressively dehydrated in a graduated series of ethanol solutions and embedded in epoxy resin. Finally, ultrathin sections (70 nm) were stained with 2% uranyl acetate and lead citrate. The ultrastructure of cells was examined with a transmission electron microscope (JEOL, Japan).

Immunofluorescence staining

OVX-MSCs were treated with conditioned medium for indicated time periods. After washing by PBS, the cells were fixed with 4% paraformaldehyde for 20 min at room temperature. Cells were incubated with 5% BSA for 1 h following permeabilization with 0.5% Triton for 15 min. For protein detection and localization, the cells were incubated with specific primary antibodies LC3b (1 μg/mL, Abcam), P62 (1:800, CST), APC (1:50, Santa Cruz) and active β-catenin (1:800, CST) overnight. After rinsing, cells were incubated with fluorescent secondary antibodies for 1 h, and counterstained with DAPI for 5 min. The images were captured by a Nikon fluorescence microscope or confocal microscope. The Pearson's colocalization coefficient between red and green fluorescence intensities was determined in 6 cells from three independent experiments using ImageJ software.

Assessment of autophagosome turnover

Cells were transfected with an mRFP-GFP tandem fluorescently tagged LC3 adenoviral vector (HanBio Techonology, Shanghai, China), according to the manufacturer's instructions. After infection, MSCs were incubated in medium containing genistein or genistein+Baf-A1 for 36 h. In green and red-merged images, yellow puncta (i.e., RFP^+GFP^+) indicates autophagosomes, while red puncta (i.e., RFP^+GFP^-) indicates autolysosomes. Both yellow and red puncta increased in cells indicating the autophagic flux was increased. Only yellow puncta is increased without red puncta alteration, or both yellow and red puncta are decreased in cells, indicating autophagic flux is blocked.

Quantitative real-time PCR analysis

Total RNA was extracted from cells with TRIzol reagent (Invitrogen, Carlsbad, CA, USA), and 1 μg of total RNA was reverse transcribed using the PrimeScript RT reagent kit (Takara Bio, Japan) according to the manufacturer's protocol. Quantitative Real-time PCR analyses were performed using the SYBR Green PCR Master Mix (TaKaRa) and detected using a Roche Light Cycler 480 (Roche Diagnostics GmbH, Germany). Each reaction was performed in triplicate and was repeated three times. The $2^{-\Delta\Delta CT}$ method was used to quantify the mRNA expression of the genes: runt-related transcription factor 2 (Runx2), bone morphogenetic protein 2 (Bmp2), type I collagen α (Col1α), bone sialoprotein (Bsp), osteocalcin (Ocn), catenin beta 1 (Ctnnb1), adenomatous

polyposis coli (APC), Axin2 and Cyclin D1. The primer sequences performed in this study are listed in Supplementary Table S1.

Western blot assay

Cell extracts were collected and quantified using BCA Protein Assay Kit (Beyotime). Protein lysate was loaded onto 10%–15% SDS-PAGE and then transferred to PVDF membranes (Millipore, Billerica, USA). Membranes were blocked in 5% fat-free milk for 2 h and then incubated with primary antibodies at 4 °C overnight. Subsequently, the membranes were incubated with secondary antibodies for 1 h, and the blotted bands were visualized by chemiluminescence detection system (Millipore). Quantitative analysis of the Western blot was carried out using ImageJ software. The primary antibodies were used as follows: anti-LC3b (1:2000, Abcam), anti-P62 (1:2000, Abcam), anti-APC (1:1000, Abcam), anti-Runx2 (1:1000, Abcam), anti-Bmp2 (1:1000, Abcam), anti-Axin2 (1:1000, Abcam), anti-CK1α (1:1000, Santa Cruz Biotechnology), anti-TFEB (1:1000, Invitrogen), antibodies from CST (anti-LC3b, anti-β-catenin, anti-active-β-catenin, anti-Dvl2, anti-GSK-3β, anti-p-GSK-3β, anti-Atg7, anti-Ulk1, anti-mTOR, anti-p-mTOR, anti-p-p70S6K, anti-β-actin and anti-Histone H3) were used at 1:1000 dilution.

Co-immunoprecipitation (Co-IP)

Cells were washed twice with ice cold PBS and lysed on ice in IP lysis/wash buffer (Pierce) supplemented with protease inhibitor (Pierce) for 15 min. After centrifugation (10 min, 15,000 × *g*, 4 °C), supernatants were collected and normalised to the protein content. For Co-IP studies, generally 10 µL of antibody was added to a volume of 500 µL with 800 µg protein. Control IPs were done with same amounts of purified rabbit IgG. After incubation overnight at 4 °C, samples were incubated with protein A/G magnetic beads (Pierce) for 1 h at room temperature with constant rotation. Immunocomplexes were washed with IP lysis/wash buffer for three times and solved by heating for 10 min at 100 °C in lane marker sample buffer (Pierce) for subsequent immunoblot assay.

Statistical analysis

Statistical tests were performed using the GraphPad prism (Version 9.0, GraphPad Software, San Diego, CA, USA). Values were presented as mean ± SD. The numerical data in different groups were tested by analysis of variance (ANOVA), and Tukey's multiple comparison test was used as a post hoc test. When only 2 groups were compared, an unpaired Student's *t*-test was used, unless otherwise stated. *P*-value < 0.05 was taken as statistical significance.

RESULTS

Genistein inhibits bone loss and bone-fat imbalance in ovariectomized rats

At the end of in vivo experiment, serum levels of the bone formation marker b-ALP and bone resorption marker CTX were significantly higher in the OVX groups than in the Sham groups ($P < 0.01$). The administration of genistein significantly upregulated the b-ALP level and downregulated CTX level in the OVX groups (Fig. 1a).

Then we analyzed the effect of genistein on ovariectomy-induced bone loss. Compared with Sham group, the micro-CT images of the distal femur showed an apparent bone loss in the ovariectomized rats (Fig. 1b). Eight weeks of genistein treatment significantly reversed bone loss in the ovariectomized rats (Fig. 1b). Compared with OVX + VEH group, a significant increase of total BMD, BV/TV and Tb.Th., as well as a decrease of Tb. Sp. was observed in the OVX + GEN group (Fig. 1c). Micro-CT analyses also showed that genistein alone did not affect trabecular bone when bilateral ovaries were not removed (Fig. 1b, c). Histomorphometric analyses showed that the mineral appositional rate and the bone formation rate were significantly higher in OVX groups compared to Sham groups (Fig. 1d, e). Genistein treatment stimulated bone formation in OVX rats but had no effect in Sham rats (Fig. 1d, e). Also, histology of the femur samples displayed a partially restored architecture of trabecular bone in ovariectomized rats treated with genistein (Fig. 2a).

To investigate the autophagy activity of MSCs in vivo, we examined LepR and P62 expression in the trabecular bone area of distal femur sections. Recent work from the Morrison laboratory has demonstrated that MSCs in adult bone marrow specifically express the leptin receptor (LepR) [22]. P62 serves as an index of autophagic degradation as it is incorporated into the completed autophagosome and then degraded in autolysosomes when autophagy occurs [23]. Double immunofluorescence labeling revealed that the $LepR^+$ cells positive for P62 in Sham groups were significantly outnumbered by the OVX + VEH group (Fig. 2b). Genistein treatment markedly reduced the P62 expression of $LepR^+$ cells in the femurs of OVX rats. Interestingly, we observed clusters of P62 dots in the $LepR^+$ cells from OVX + GEN group, indicating the formation of autophagic vesicles (Fig. 2b, white arrowhead).

Immunohistochemical staining demonstrated that compared to Sham groups, the Ocn (marker of mature osteoblast) and Fabp4 (marker of adipocyte) protein signals increased in femurs of OVX + VEH group (Fig. 2c, d). Notably, compared to the OVX + VEH group, genistein administration enhanced the percentage of Ocn-positive mature osteoblasts and suppressed the percentage of Fabp4-positive adipocytes in the distal femur (Fig. 2c, d), indicating a rebalance of dysregulated osteoblast-adipocyte lineage commitment of OVX-MSCs. Also, genistein treatment led to a decrease in the osteoclast number in the OVX group (Fig. 2e, f).

Effects of genistein on proliferation, lineage commitment and autopahgy in OVX-MSCs

OVX-MSCs express high levels of typical MSC markers including CD44 and CD90, and lack expression of CD45 and CD31 (Fig. 3a). Exposure of OVX-MSCs to 1–1000 nM genistein for 7 days had no effect on cell viability (Fig. 3b).

As normal bone homeostasis relies on the dynamic balance between osteogenesis and adipogenesis in differentiating MSCs, we assessed phenotypical changes of OVX-MSCs cultured with genistein at different concentrations. Upregulation of mineralization level was observed in 1, 10, and 1000 nM genistein groups (Fig. 3c), and the 10 nM genistein treatment led to the maximal effect on ALP activity (Fig. 3c, d). During the genistein treatment, the mRNA and protein expression of the master osteogenic transcription factors Runx2 and Bmp2 were significantly upregulated (Fig. 3e, f). As a result, osteogenesis marker genes Bsp, Col1α and Ocn were notably upregulated at the mRNA level (Fig. 3g). It is noticeable that, during the period of treatment, 10 nM of genistein led to the maximal enhancement on expression of osteogenesis transcription factors and osteogenesis marker genes (Fig. 3e–g).

We further examine the effect of 10 nM genistein on the adipogenic differentiation of OVX-MSCs. The result of Oil-Red-O staining showed that the administration of 10 nM genistein for 3 days before the adipogenic induction could markedly decrease the number and size of pre-adipocytes (Fig. 3h). We also analyzed the mRNA expression of the adipocytic transcription factors nuclear receptor peroxisome proliferator-activated receptor-γ (Pparg), CCAAT/enhancer binding protein α (Cebpa), and adipocyte markers including Fabp4 and lipoprotein lipase (Lpl). Consistently, 10 nM genistein significantly inhibited the expression of markers of adipocyte differentiation (Fig. 3i). These findings demonstrated that an inverse regulation between increasing osteogenic differentiation and decreasing adipogenic differentiation by 10 nM genistein treatment.

Given the role of autophagy in regulating stem cell differentiation [24, 25], we detected the formation of autophagic elements

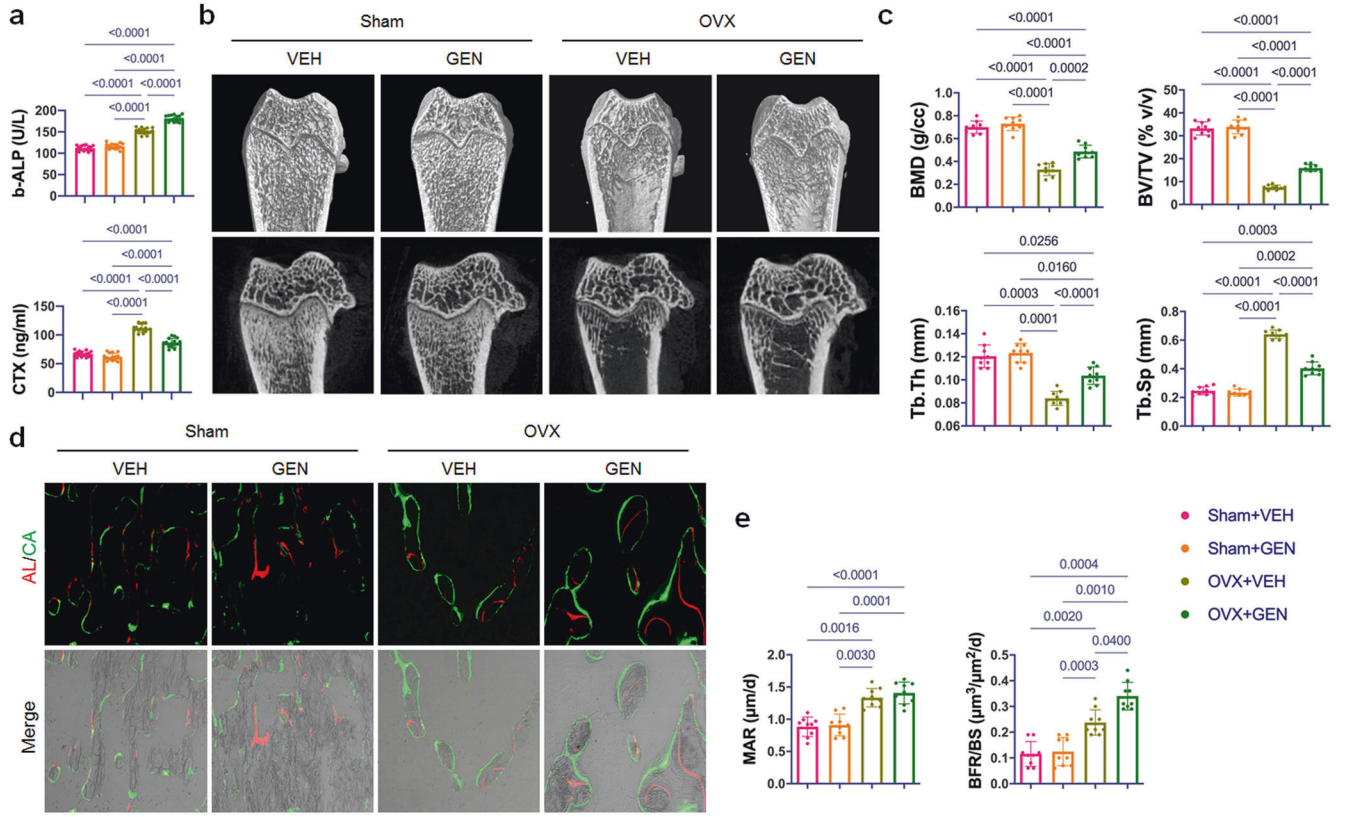

Fig. 1 Genistein treatment prevented trabecular bone loss and promoted cancellous bone formation in ovariectomized rats. a Effect of genistein on serum bone-alkaline phosphatase (b-ALP) and collagen C-telopeptides (CTX) ($n = 15$/group). **b** Representative micro-CT images of femoral trabecular bone. Upper panel: 3-D reconstruction; lower panel: 2-D image. **c** Quantitative analyses of the bone mineral density (BMD), bone volume per tissue volume (BV/TV), trabecular thickness (Tb.Th), and trabecular separation (Tb.Sp) of femoral trabecular bone ($n = 9$/group). **d** Representative images of Alizarin Red S and calcein labeled tibial trabecular bone, which showed the structural and dynamic changes in the tibia from OVX rats after different treatments. **e** Dynamic histomorphometric analysis of mineral apposition rate (MAR) and bone formation rate (BFR/BS) in tibial trabecular bone ($n = 9$/group). Data were shown as means with SD, and all data points. One-way ANOVA followed by Tukey post hoc test was used in **a**, **c**, and **e**.

and autophagic flux in OVX-MSCs treated by 10 nM genistein. Autophagic flux is often assessed by Western blot, which detects LC3b-II in the absence and presence of autophagy inhibitor, and examines the autophagy-dependent degradation of appropriate substrates such as P62. The result of Western blot showed increased LC3b-II level and decreased P62 expression in OVX-MSCs treated with genistein for 48 h (Fig. 3j). Baf-A1 is an autophagy inhibitor that can prevent autolysosome degradation. If autophagy flux is occurring, the amount of LC3b-II will be higher in the presence of Baf-A1. Compared to the genistein group, the LC3b-II level was higher in the genistein+Baf-A1 group (Fig. 3j). The result of Western blot indicated that the genistein induced the autophagic flux in OVX-MSCs. To further confirm the effect of genistein on autophagy, we monitored the autophagic flux using the mRFP-GFP-LC3 reporter. The mRFP-GFP-LC3 fluorescence assay is designed to monitor autophagic flux, based on the fact that GFP signal is sensitive to the acidic condition of the lysosome lumen, while the mRFP signal has no significant change under the acidic condition. Autophagic flux is increased when both yellow and red puncta are increased in cells, while autophagic flux is blocked when only yellow puncta are increased without red puncta alteration, or when both yellow and red puncta are decreased in cells. Fluorescence microscopy showed that genistein significantly increased GFP-LC3 and RFP-LC3 puncta in OVX-MSCs, and the co-culture with Baf-A1 increased GFP/RFP co-localization, demonstrating an increased autophagic flux in cells by genistein treatment (Fig. 3k). Transmission electron microscopy was performed and showed an increase in the formation of autophagic vesicles in OVX-MSCs treated by genistein (Fig. 3l). These results demonstrated that 10 nM genistein activated autophagy in OVX-MSCs.

Collectively, our data indicated that 10 nM genistein promoted osteoblastic differentiation and activated autophagy in OVX-MSCs.

Genistein promotes osteoblastic differentiation of OVX-MSCs via enhancing autophagic activity

The aforementioned data implied that autophagy might be involved in the osteoblastic differentiation effect of genistein on OVX-MSCs. To test this hypothesis, we used autophagy inhibitor Baf-A1 and Atg7/Ulk1 knockdown, to determine whether autophagy indeed plays an important role in osteoblastic differentiation of OVX-MSCs.

Pharmacological inhibition of autophagy by Baf-A1 effectively inhibited the genistein-stimulated ALP activity and alizarin red staining-positive nodules, as shown in Fig. 4a, b. However, Baf-A1 is not specific autophagy inhibitor, the result should be interpreted with caution. Long-term treatment of Baf-A1 can cause significant disruption of the mitochondrial network in cultured cells [26]. Genetic knockout or knockdown of autophagy genes is indispensable to exclude the possibility that the observed phenotype is due to the side effect of Baf-A1.

Activation/assembly of the Ulk1 complex in mammals is one of the first steps in autophagy induction [23], and Atg7 is one of the essential elements in phagophore elongation and LC3 lipidation. Efficient knockdown of Atg7 and Ulk1 in cells were confirmed by qRT-PCR (Supplementary Fig. S1a) and Western blot (Fig. 4c–f). Western blot analysis showed that 72% of Atg7 protein and 69%

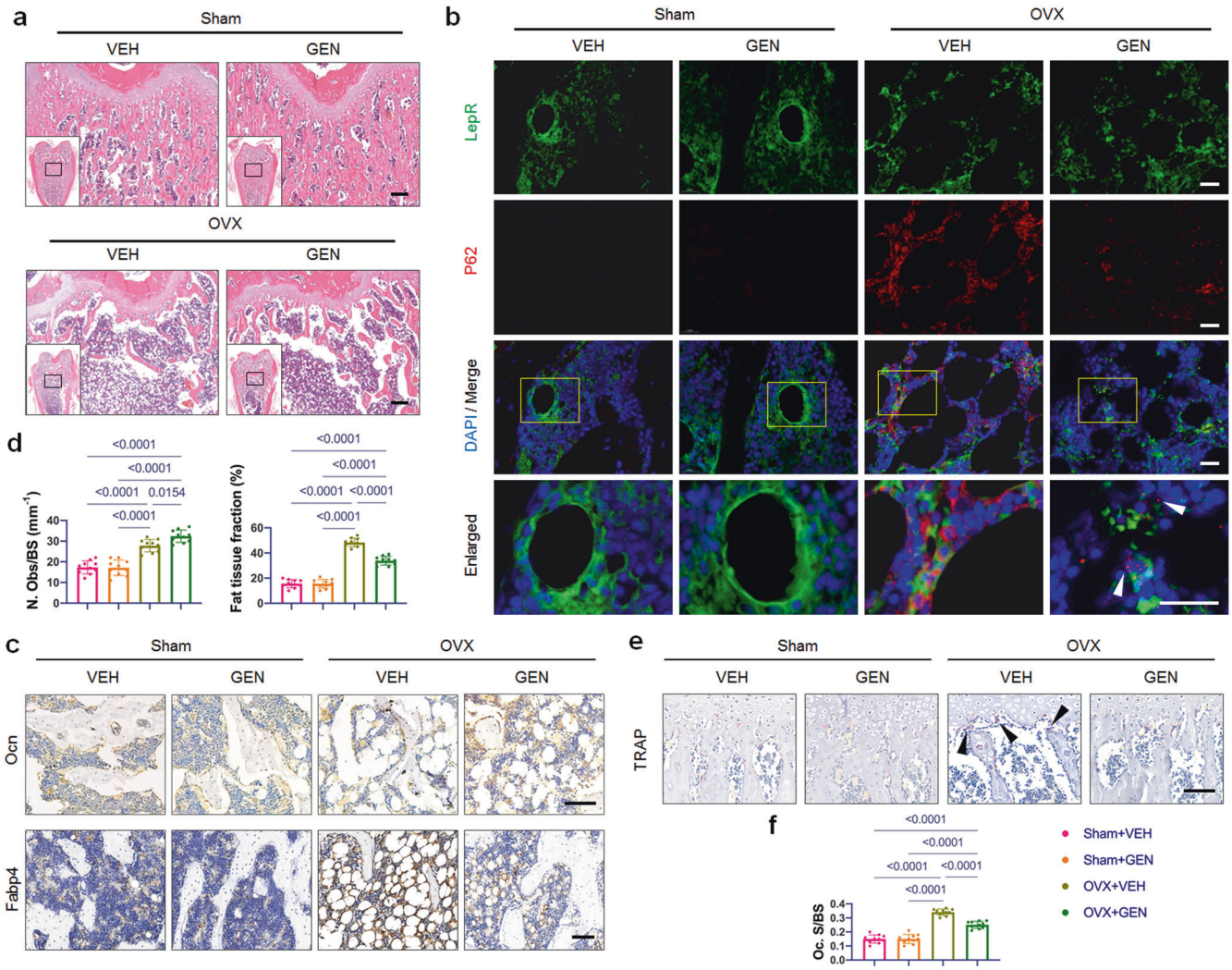

Fig. 2 Genistein treatment reversed trabecular bone loss and abnormal autophagy induced by ovariectomy. a Representative images of H&E-stained distal femur sections. Scale bar, 200 μm. **b** Representative images of double immunofluorescence labeling of P62 and LepR at the bone marrow area of distal femur. Yellow boxes indicate the area of high magnification on the up panel. White arrowheads indicate the dots of P62. Scale bar, 20 μm. **c** Representative images of immunohistochemistry for Ocn and Fabp4. Scale bar, 100 μm. The results of quantitative measurements of osteoblasts and fat tissue are presented on (**d**) ($n = 10$/group). N. Obs/BS, number of osteoblasts per bone surface. **e**, **f** TRAP staining and quantification of Oc.S/BS (osteoclast surface per bone surface). Black arrowheads indicate osteoclasts. Scale bar, 100 μm. $n = 10$/group. Data were shown as means with SD, and all data points. One-way ANOVA followed by Tukey post hoc test was used in **d** and **f**.

of Ulk1 protein was depleted in OVX-MSCs transfected with Atg7 siRNA and Ulk1 siRNA, respectively. The decreased level of LC3-II and increased level of P62 protein demonstrated that the autophagic machinery was inhibited by Atg7 and Ulk1 knockdown (Fig. 4c–f). Moreover, the autophagy activation induced by genistein was suppressed by Atg7 and Ulk1 knockdown (Fig. 4c–f). Consistent with the inhibited autophagy, the genistein-induced osteoblastic differentiation of OVX-MSCs was also remarkably suppressed by Atg7 or Ulk1 knockdown, as shown by the decreased ALP activity and mineral content (Fig. 4g, h). The reduced mRNA levels of Bsp, Col1α and Ocn also indicated that the osteoblastic differentiation effect of genistein on OVX-MSCs was inhibited by Atg7 or Ulk1 knockdown (Fig. 4i). In conclusion, genistein may promote osteoblastic differentiation of OVX-MSCs via autophagy activation.

Genistein-induced autophagy activates canonical Wnt/β-catenin signaling pathway

Wnt/β-catenin signaling pathway plays a pivotal role in the initiation of osteoblast differentiation of mesenchymal progenitor cells [16]. Prolonged exposure to Wnt/β-catenin signaling inhibited late-stage osteoblastic differentiation and the formation of mineralized matrix [27]. To explore the potential molecular mechanism, we analyzed the canonical Wnt/β-catenin signaling pathway during 72 h course of genistein treatment. The protein level of total β-catenin, active non-phosphorylated β-catenin were significantly upregulated at 36 and 48 h of genistein treatment, then reduced at 72 h (Fig. 5a). However, the mRNA expression of Ctnnb1, the gene encoding β-catenin, was not changed (Fig. 5b). Immunofluorescent staining showed that genistein also induced nuclear translocation of active β-catenin (Fig. 5c). As a consequence of β-catenin signaling activation, the mRNA expression of β-catenin downstream target genes, such as Axin2 and Cyclin D1, were also increased during 48 h of genistein treatment (Fig. 5b). To further clarify the relationship between genistein-induced β-catenin upregulation and osteoblastic differentiation, we inhibited β-catenin expression by si-ctnnb1 in OVX-MSCs. As expected, knockdown of ctnnb1 significantly inhibited the osteoblastic differentiation effect of genistein on OVX-MSCs, as shown by the decreased ALP and ARS staining (Fig. 5d). These results indicated

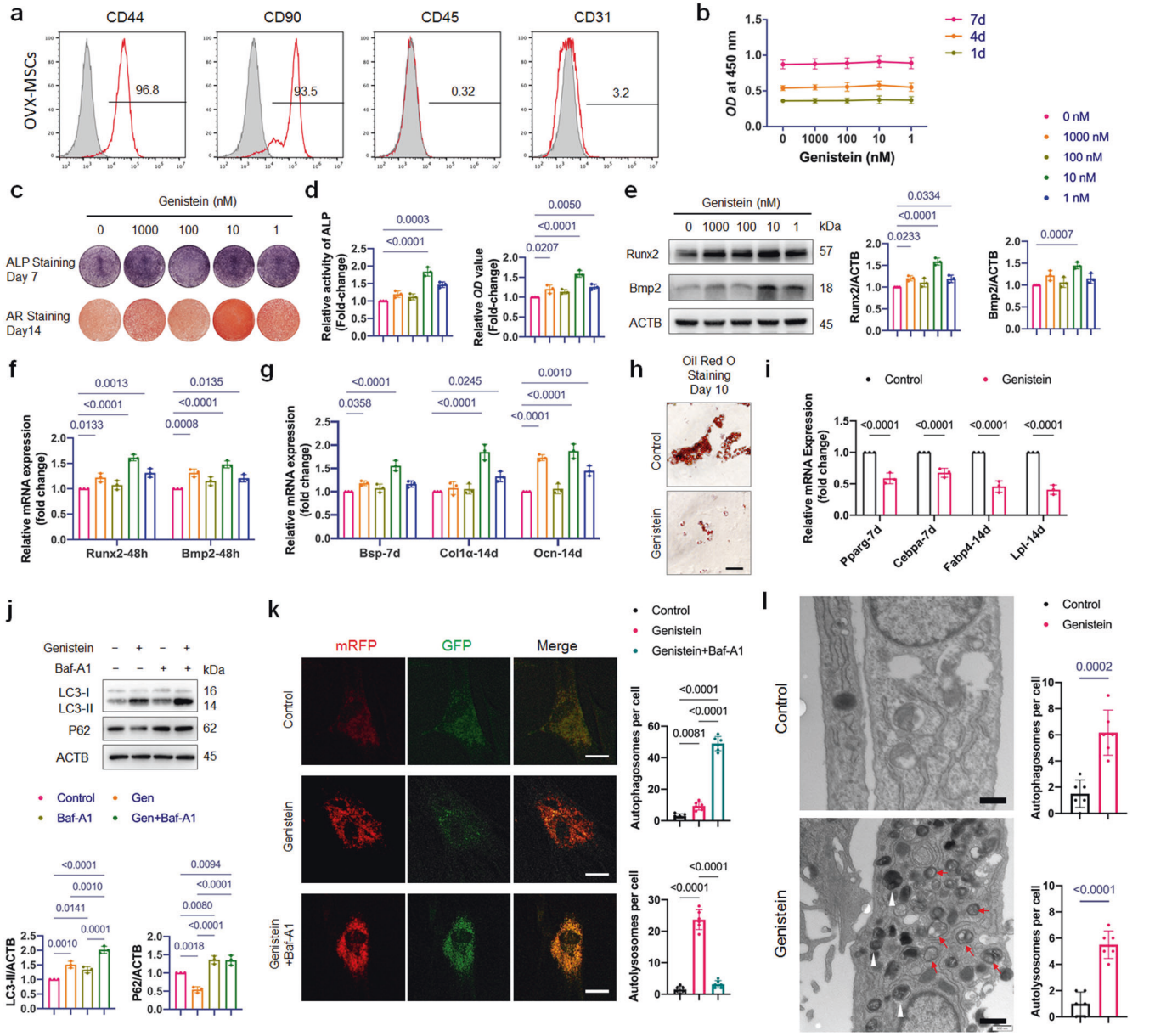

Fig. 3 Effects of genistein on proliferation, lineage commitment and autophagy of OVX-MSCs. a Flow cytometric analysis of cell surface markers on OVX-MSCs. The gray histogram represented isotype control cells and the red histogram represented the cells incubated with the indicated antibodies (CD44, CD90, CD45 and CD31). **b** The effect of genistein at different concentrations (1–1000 nM) on the proliferation of OVX-MSCs was evaluated ($n = 3$). **c**, **d** OVX-MSCs were treated with genistein at different concentrations (1–1000 nM) for 48 h, then cultured in osteogenic medium for the indicated time periods. ALP staining and Alizarin Red staining, as well as ALP activity assays and quantitative analysis of the Alizarin Red staining were performed ($n = 3$). Genistein significantly increased ALP activity and bone nodule formation in OVX-MSCs. **e** Western Blot assay was performed to detect the Runx2 and Bmp2 expression in OVX-MSCs treated by genistein for 48 h. Representative Western blots and densitometric quantifications are shown ($n = 3$). **f** Real-time qPCR assay was performed to examine changes in the mRNA expression of the master osteogenic transcription factors including Runx2 and Bmp2 ($n = 3$). **g** Real-time qPCR assay was performed to examine changes in expression of osteoblastic differentiation marker genes including Bsp, Col1α and Ocn ($n = 3$). **h**, **i** OVX-MSCs were treated with or without 10 nM genistein for 3 days, then cultured in adipogenic inducing medium for the indicated time periods. The results of Oil-Red-O staining and qRT-PCR showed that the genistein significantly inhibited adipogenesis of OVX-MSCs ($n = 3$). Scale bar, 100 μm. **j** OVX-MSCs were treated by genistein in the presence or absence of bafilomycin A1 (Baf-A1, 10 nM) for 48 h, Western blot analysis was performed to detect the LC3-II and P62 expression. Representative Western blots and densitometric quantifications are shown ($n = 3$). **k** Representative confocal images of OVX-MSCs transfected with lentivirus containing mRFP-GFP-LC3 construct. Cells were treated with genistein in the presence or absence of Baf-A1 for 36 h. Red puncta (i.e., RFP^+GFP^-) indicated autolysosomes, and yellow puncta (i.e., RFP^+GFP^+) indicated autophagosomes. Quantitative measurements of autolysosomes and autophagosomes are shown on right ($n = 6$ cells/group). Scale bar, 20 μm. **l** Autophagic vacuoles were observed by transmission electron microscopy in cells treated with genistein for 36 h. Red arrows indicate typical autophagosomes, which characterized by 2 bilayers separated by a narrow electron-lucent cleft. White arrowheads indicate autolysosomes, which can be identified as one limiting membrane structure containing electron dense cytoplasmic material and/or organelles at various stages of degradation. Scale bar, 500 nm. Statistical analysis was performed to calculate the number of autophagosomes and autolysosomes in cells ($n = 6$ cells/group). Data were shown as means with SD, and all data points. One-way ANOVA followed by Tukey post hoc test was used in **b**, **d**, **e**–**g**, **j**, and **k**. Unpaired Student's *t*-test was used in **i** and **l**.

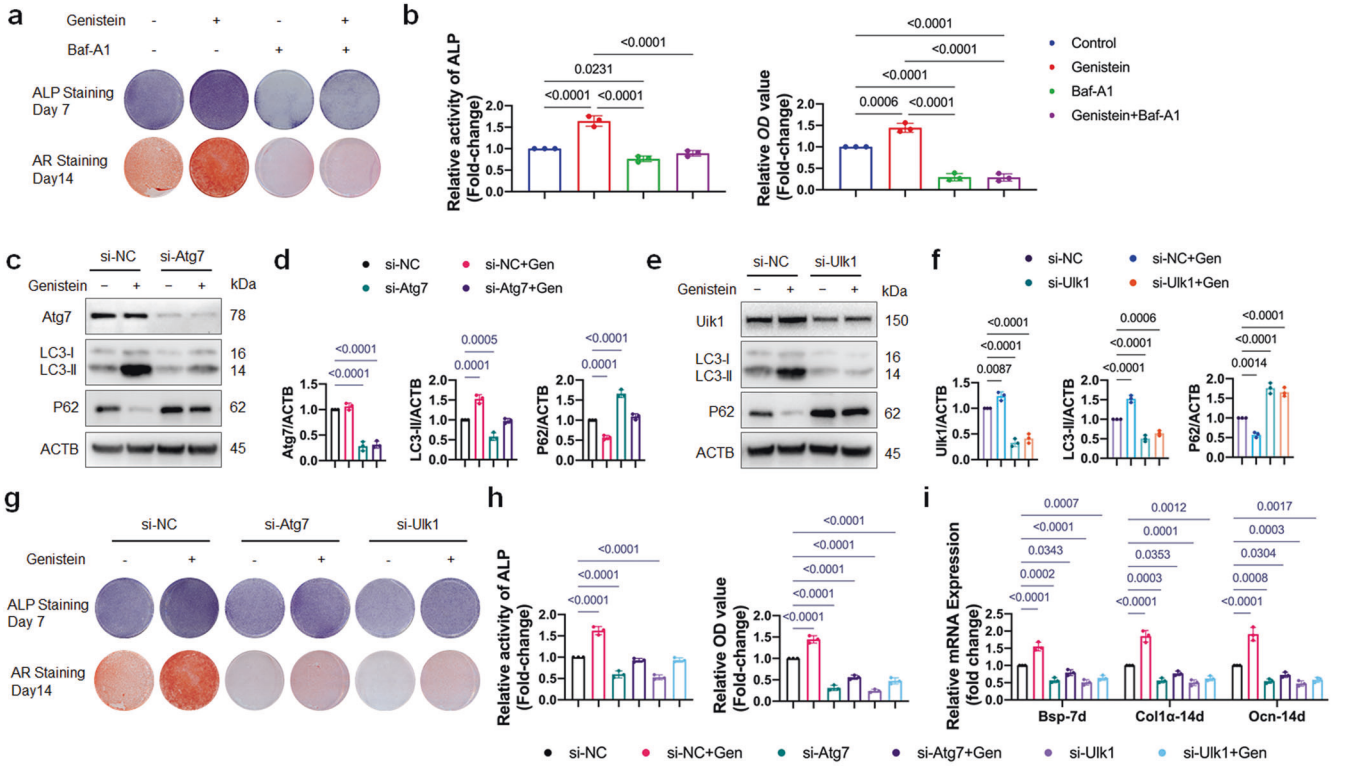

Fig. 4 Autophagy induction is required for genistein-mediated osteoblastic differentiation and Wnt/β-catenin signaling activation. **a**, **b** OVX-MSCs were incubated with genistein without or with Baf-A1 for 48 h, then cultured in osteogenic medium for the indicated time periods. ALP staining and Alizarin Red staining, as well as ALP activity assays and quantitative analysis of the Alizarin Red staining were performed ($n = 3$). **c**–**f** The protein expressions of Atg7, Ulk1, LC3, and P62 were assessed by Western blot. Representative Western blots and densitometric quantifications are shown ($n = 3$). OVX-MSCs were transfected with Atg7 or Ulk1 siRNAs, and subsequently treated with genistein for 48 h. **g**, **h** OVX-MSCs were transfected with Atg7 or Ulk1 siRNAs, then treated with genistein for 48 h, followed by the osteogenic medium stimulation for the indicated time periods. ALP staining at day 7 and Alizarin Red S staining at day 14 were performed. ALP staining and Alizarin Red staining, as well as ALP activity assays and quantitative analysis of the Alizarin Red staining were performed ($n = 3$). **i** Real-time qPCR assay was performed to examine changes in expression of osteoblastic differentiation marker genes including Bsp, Col1α and Ocn ($n = 3$). Data were shown as means with SD, and all data points. One-way ANOVA followed by Tukey post hoc test was used in **b**, **d**, **f**, **h** and **i**.

that genistein-induced β-catenin stabilization and accumulation indeed contributed to the osteoblastic differentiation of OVX-MSCs.

An important question remains to be answered is whether or not genistein upregulate β-catenin level through autophagy pathway. To address this question, we co-culture OVX-MSCs with genistein in the presence of Baf-A1 for 48 h. The result showed that Baf-A1 completely blocked genistein-induced upregulation of active β-catenin level (Fig. 5e), as well as the upregulation of the mRNA levels of Axin2 and Cyclin D1 (Fig. 5f). Moreover, the upregulation of active β-catenin protein level and mRNA expression of Axin2 and Cyclin D1 induced by genistein treatment was also attenuated by knockdown of Atg7 or Ulk1 in OVX-MSCs (Fig. 5g, h). Taken together, these data suggested that genistein-induced autophagy promoted β-catenin upregulation by unknown mechanism.

Genistein stabilizes β-catenin through autophagy-dependent APC degradeation

The master regulator of canonical Wnt pathway is the cytoplasmic protein β-catenin. Its stability is controlled by the destruction complex, which is formed by core proteins APC, Axin, GSK-3β, and CK1α. In addition, dishevelled protein 2 (Dvl2) palys an important role in canonical Wnt signaling [28]. We then explored which mediator of Wnt signaling might undergo down-regulation by genistein-induced autophagy. As show in Fig. 6a, the protein level of APC was remarkably decreased at 36 and 48 h of genistein treatment, while the protein level of GSK-3β, p-GSK-3β, CK1α and Dvl2 were not affected. In contrast, the Axin2 expression increased due to the Wnt signaling activation. The mRNA expression of Ctnnb1/β-catenin and Apc did not change during genistein treatment in the presence or absence of Baf-A1 for 48 h (Supplementary Fig. S1b), suggested that the observed decrease of APC protein expression was through post-translational rather than transcriptional regulation. In the presence of protein synthesis inhibitor, cycloheximide, the degradation of APC protein was accelerated (Fig. 6b), suggesting that genistein downregulated APC protein by promoting APC degradation. There are two major protein degradation systems in eukaryotic cells: the ubiquitin-proteasome system (UPS) and autophagy [29]. We next investigated which system dominantly mediates the degradation of APC by genistein. We found that the genistein-induced decrease in APC protein expression was rescued by the autophagy inhibitor Baf-A1, but not the proteasome inhibitor MG132 (Fig. 6c). Moreover, knockdown of Atg7 and Ulk1 reversed the down-regulation effect of genistein on APC protein level (Fig. 6d), provided direct evidence that genistein stimulated autophagic degradation of APC. These data together suggested that autophagy positively regulates Wnt signaling by autophagic degradation of APC.

To assess whether APC is recruited to the autophagosomes, immunofluorescence microscopy examination was performed. Under normal growth conditions, APC and LC3 were diffused in the cytoplasm. During genistein treatment, we observed clusters of APC dots co-localized with endogenous LC3 puncta, and this APC-LC3 co-localization was further increased by co-culture with

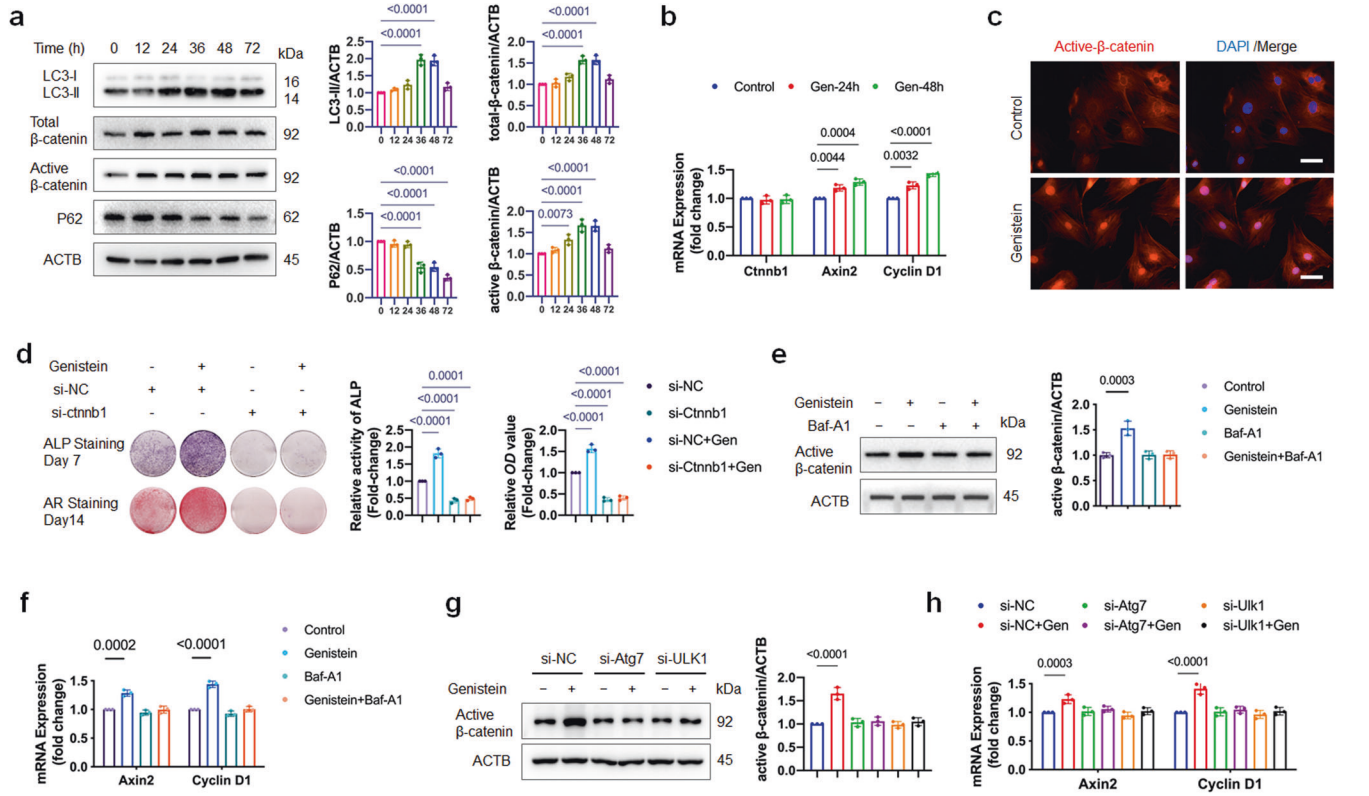

Fig. 5 Genistein-induced autophagy activates canonical Wnt/β-catenin signaling pathway. a OVX-MSCs were treated with genistein and assayed for changes in LC3-II, P62, total β-catenin and active β-catenin expression over a 72 h window. The graphs on the right show quantifications of the protein expression level normalized to ACTB ($n = 3$). **b** qRT-PCR was performed to examine changes in expression of Ctnnb1/β-catenin and Wnt-target gene Axin2 and Cyclin D1 during 48-h of genistein treatment ($n = 3$). **c** Genistein induced nuclear translocation of active β-catenin after 48 h treatment ($n = 3$). Representative images are shown. Scale bar, 50 μm. **d** OVX-MSCs were transfected with control or ctnnb1 siRNA, then treated with genistein for 48 h, followed by osteogenic medium stimulation for the indicated time periods. ALP staining and Alizarin Red staining, as well as ALP activity assays and quantitative analysis of the Alizarin Red staining were performed ($n = 3$). **e**, **f** OVX-MSCs were incubated with genistein with or without Baf-A1 for 48 h. Representative Western blots and densitometric quantifications of active β-catenin are shown ($n = 3$). The mRNA levels of Wnt target gene Axin2 and Cyclin D1 were analyzed by qRT-PCR ($n = 3$). **g**, **h** OVX-MSCs were transfected by Atg7 or Ulk1 siRNA, then treated with 10 nM genistein for 48 h. Representative Western blots and densitometric quantifications of active β-catenin are shown ($n = 3$). qRT-PCR was performed to detect the mRNA expression of Axin2 and Cyclin D1 ($n = 3$). Data were shown as means with SD, and all data points. One-way ANOVA followed by Tukey post hoc test was used in **a**, **b**, **d**–**h**.

Baf-A1 (Fig. 6e, f). The co-localization of APC with LC3 suggests that these two proteins may interact with each other in the cytoplasm. Since P62/SQSTM1 is the dominant autophagic substrate which recruits protein aggregates to autophagosomes for degradation [30], we also performed the immunofluorescence microscopy examination of APC and P62. Conversely, poor colocalization of P62 and APC was observed (Fig. 6g, h). LC3 is known to bind to cargoes targeted for selective turnover in autophagosomes [31]. Co-immunoprecipitation revealed that APC interacted with LC3 at the endogenous level in OVX-MSCs, and this interaction was significantly increased under genistein treatment (Fig. 6i). Co-culture with Baf-A1 could further increase the APC-LC3 interaction (Fig. 6i). Collectively, the above results demonstrated that APC interacts with LC3 and hence is specifically degraded by autophagy.

We were interested whether other plant polyphenols could affect APC by autophagy. Resveratrol and quercetin were both reported to promote osteoblast differentiation in osteoporotic MSCs [32, 33]. In vitro working solutions were set at 10 μM for resveratrol and 1 μM for quercetin according to previous studies [32, 34], and autophagy flux was determined by measuring the LC3-II and P62 in the absence and presence of lysosomal inhibitor Baf-A1. Similar to genistein, resveratrol activated autophagy, upregulated active-β-catenin level and downregulated APC level in OVX-MSCs (Fig. 6j, k). On the contrary, no significant changes in the autophagy, active-β-catenin and APC level were observed by quercetin treatment (Fig. 6j, l).

TFEB upregulation is involved in genistein-activated autophagy

Subsequently we investigated the upstream regulators that mediate the activation of autophagy by genistein. To explore if the inhibition of mammalian target of rapamycin (mTOR) is involved or not, we assessed the protein level of mTOR and its downstream target p70S6K. Surprisingly, no significant changes in the phosphorylation of mTOR or its downstream factors were observed (Fig. 7a). However, we found that the protein level and nuclear translocation of TFEB were enhanced by genistein treatment (Fig. 7b, c), and the lysosomal marker lysosome-associated membrane protein 2 (LAMP2, one of the TFEB targeted genes) was also increased in genistein-treated cells (Fig. 7a). Together, these results suggested that TFEB, rather than mTOR, may be involved in the activation of autophagy by genistein.

TFEB is a master transcriptional regulator of lysosomal biogenesis and autophagy, and TFEB-mediated autophagy activation often leads to increase in Beclin 1 (Becn1) and Atg5 level to facilitate the autophagy initiation [35]. To confirm the role of TFEB in genistein-activated autophagy, we knocked down TFEB by siRNA in OVX-MSCs. We found that genistein showed much less effect on

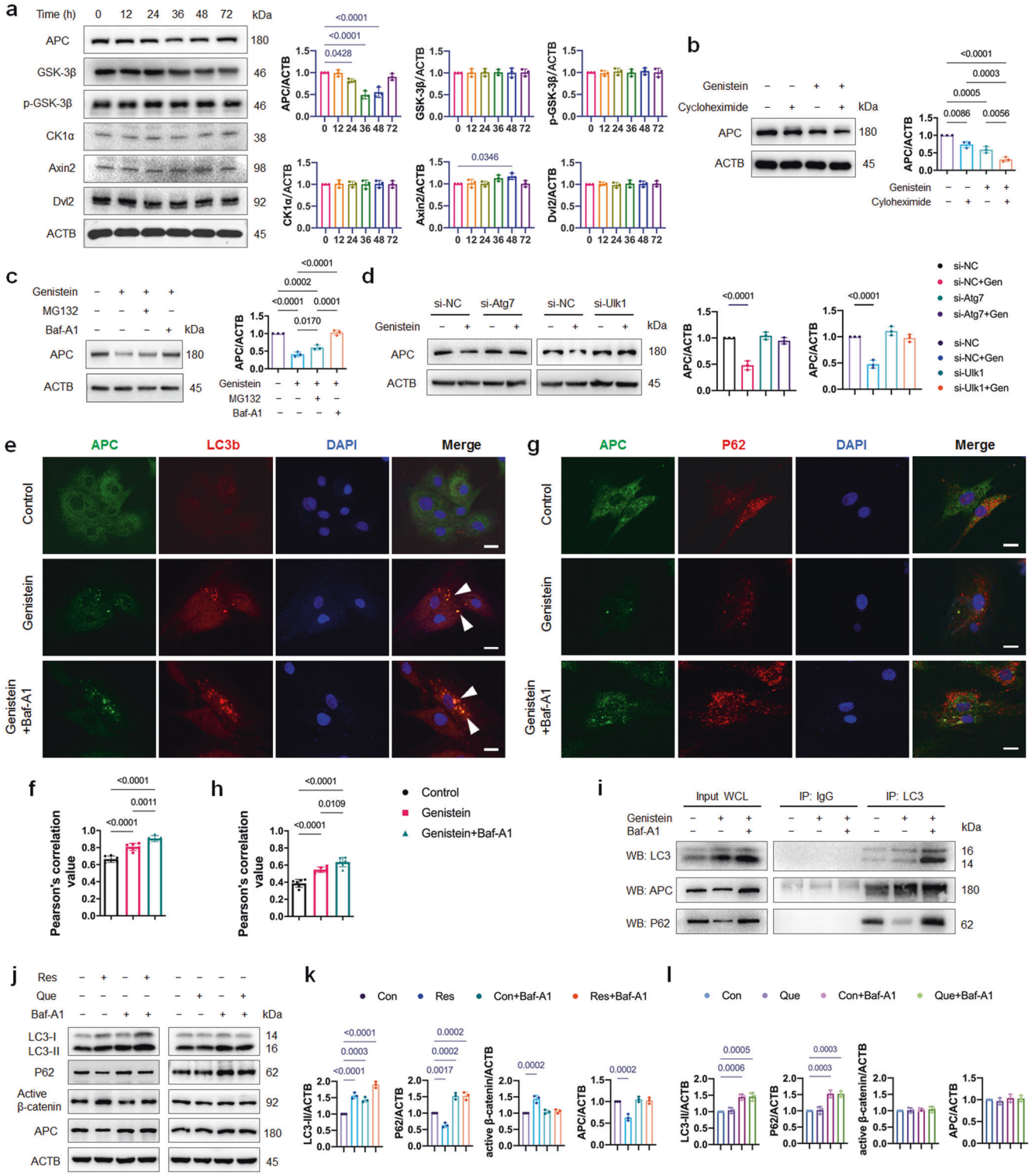

autophagy activation and Atg5 and Becn1 upregulation in TFEB depleted cells than in control cells (Fig. 7d), confirming that TFEB is the major upstream regulator of genistein-activated autophagy.

Based on our findings, we proposed a working model to illustrate the mechanism (Fig. 7e): during genistein treatment, the APC aggregates are selectively fetched by LC3 into autophagosomes, followed by degradation in autolysosomes, thus the formation of destruction complex is inhibited by the downregulated APC level. As a consequence, stabilized β-catenin translocates to the nucleus, initiates the osteoblastic differentiation of OVX-MSCs.

The osteogenesis promoting effect of genistein on healthy-MSCs was independent of autophagy

Various studies have reported that genistein could stimulate osteogenic differentiation of MSCs in vitro [10–13]. In order to

Fig. 6 Genistein upregulates active β-catenin protein level through autophagic degradation of APC. a OVX-MSCs were treated with genistein and assayed for changes in expression of Wnt signaling mediators over a 72 h window. The graphs on the right show quantifications of the protein expression level normalized to ACTB ($n = 3$). **b** OVX-MSCs were incubated with cycloheximide for 1 h, then supplemented with 10 nM genistein for 48 h. Protein expression of APC was detected by Western blot, and quantitative analysis of APC/ACTB ratio was presented ($n = 3$). **c** OVX-MSCs were treated with genistein for 48 h in the absence or presence of proteasome inhibitor MG132 and autophagy inhibitor Baf-A1. Quantitative analysis of APC/ACTB ratio was presented ($n = 3$). **d** OVX-MSCs were transfected by Atg7 or Ulk1 siRNA, and treated with genistein for 48 h. The protein expression of APC was detected by Western blot, and the quantitative analysis of APC/ACTB ratio was presented ($n = 3$). **e**–**h** OVX-MSCs were treated with genistein in the absence or presence of Baf-A1 for 48 h. Pearson's correlation value represented strength of the relationship between red fluorescence signal and green fluorescence signal ($n = 6$). Immunofluorescent images and Pearson's correlation values of LC3 and APC (**e**, **f**), as well as P62 and APC (**g**, **h**) were shown. White arrowhead indicated the APC-LC3 co-localization. Scale bar, 20 μm. **i** OVX-MSCs were treated with genistein for 36 h in the absence or presence of autophagy inhibitor Baf-A1. Co-IP study was performed to test the interaction of LC3 and APC ($n = 3$). Purified rabbit IgG was used as negative control. Left panel shows relative amounts of proteins in whole cell lysates used for Co-IP (Input). P62 was detected as a positive control. **j**–**l** OVX-MSCs were treated by resveratrol (Res, 10 μM) or quercetin (Que, 1 μM) in the presence or absence of bafilomycin A1 (Baf-A1, 10 nM) for 48 h, Western blot analysis was performed to detect the LC3-II, P62, active β-catenin and APC expression. Representative Western blots and densitometric quantifications are shown ($n = 3$). Data were shown as means with SD, and all data points. One-way ANOVA followed by Tukey post hoc test was used in **a**–**d**, **f**, **h**, **k**, **l**.

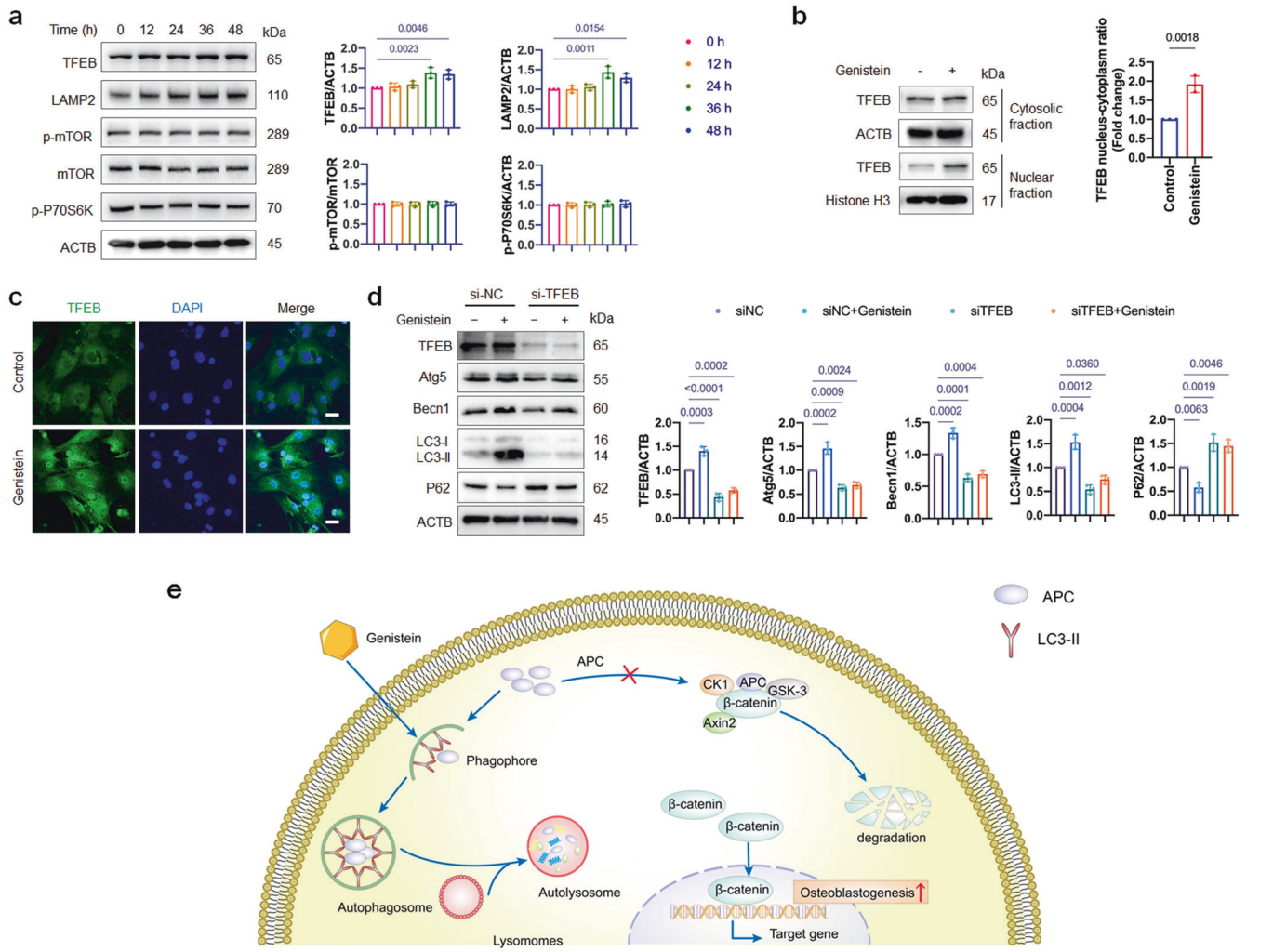

Fig. 7 TFEB upregulation is involved in genistein-activated autophagy. a Western blot assay was performed to detect the TFEB, LAMP2, mTOR, p-mTOR and p-P70S6K expression in OVX-MSCs treated by genistein for 48 h. The graphs on the right show quantifications of the protein expression level normalized to ACTB ($n = 3$). **b** Representative immunoblots showing TFEB levels in both cytosolic and nuclear fractions from cells. OVX-MSCs were treated with genistein for 36 h. Quantitative analysis of TFEB/ACTB and TFEB/Histone H3 ratio were presented ($n = 3$). **c** Representative images of immunofluorescence staining of TFEB (green) and nucleus (blue) in different groups. OVX-MSCs were treated with genistein for 36 h. **d** OVX-MSCs were transfected by TFEB siRNA, and treated with genistein for 48 h. The protein expressions of TFEB, Atg7, Becn1, LC3, and P62 were detected by Western blot, and the quantitative analysis was presented on the right ($n = 3$). **e** Working model of autophagic degradation of APC and activating of Wnt signaling pathway by genistein in OVX-MSCs. Data were shown as means with SD, and all data points. One-way ANOVA followed by Tukey post hoc test was used in **a** and **d**. Student's unpaired *t*-test was used in **b**.

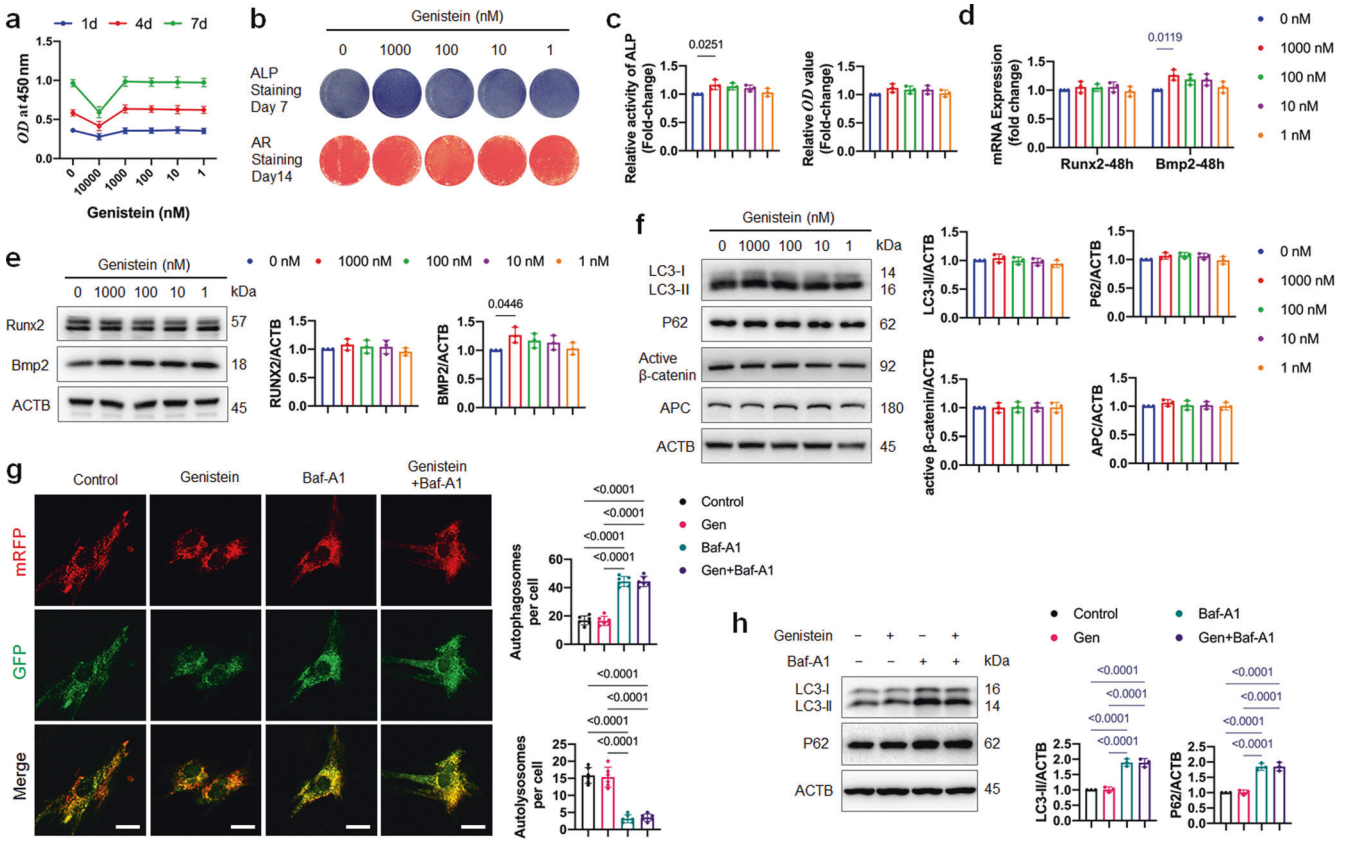

Fig. 8 Effects of genistein on proliferation, osteoblast differentiation and autophagic activity of healthy-MSCs. a The effect of genistein at different concentrations (1–10000 nM) on the proliferation of healthy-MSCs was evaluated ($n = 3$). **b**, **c** Healthy-MSCs were treated with genistein at different concentrations (1–1000 nM) for 48 h, then cultured in osteogenic medium for the indicated time periods. ALP staining and Alizarin Red S staining, as well as ALP activity assay and quantitative analysis of Alizarin Red staining were performed ($n = 3$). **d** Real-time qPCR assay was performed to examine changes of the mRNA level of Runx2 and Bmp2 in healthy-MSCs treated by genistein for 48 h ($n = 3$). **e** Western Blot assay was performed to detect the Runx2 and Bmp2 expression in healthy-MSCs treated by genistein for 48 h ($n = 3$). **f** Western blot assay was performed to detect the LC3-II, P62, active-β-catenin and APC expression in healthy-MSCs treated by genistein at different concentrations for 48 h. **g** Healthy-MSCs that expressed mRFP-EGFP-LC3 fusion protein were treated with 1000 nM genistein in the presence or absence of Baf-A1 for 48 h ($n = 6$ cells/group). Red puncta (i.e., RFP^+GFP^-) indicated autolysosomes, and yellow puncta (i.e., RFP^+GFP^+) indicated autophagosomes. Scale bar, 20 μm. **h** Healthy-MSCs were treated by 1000 nM genistein in the presence or absence of Baf-A1 for 48 h. Western blot analysis was performed to detect the LC3-II and P62 expression ($n = 3$). Data were shown as means with SD, and all data points. One-way ANOVA followed by Tukey post hoc test was used in **c**–**h**.

explore whether the above-mentioned effects are similar in healthy-MSCs, we performed experiments on MSCs derived from healthy 6-month-old female Sprague-Dawley rats. The identity of healthy-MSCs was confirmed by flow cytometry with positive staining for CD44 and CD90, but negative staining for CD45 and CD31 (Supplementary Fig. S1c). We analyzed the effect of genistein on the proliferation of healthy-MSCs, and found that 1–1000 nM genistein treated for 7 days had no effect on cell proliferation (Fig. 8a). Treatment of genistein at concentration of 10 μM significantly inhibited cell proliferation, in accordance with the literatures [36, 37] which reported that high concentration of genistein has telomerase-repressing and anti-proliferative effects. The use of 1000 nM genistein slightly but significantly up-regulated ALP protein activity (Fig. 8b, c), but no significant changes in alizarin red staining by the 1–1000 nM genistein treatments were observed (Fig. 8b, c). Further, we examined the effects of genistein on the mRNA and protein expression level of Runx2 and Bmp2. The result of qRT-PCR and Western blot showed that the expression of Bmp2 but not Runx2 increased by 1000 nM genistein treatment (Fig. 8d, e). Compared to the control group, long term administration of genistein to healthy-MSCs did not change mRNA levels of Bsp, Col1α and Ocn (Supplementary Fig. S1d). The results indicated that for healthy-MSCs, genistein only transiently promoted the osteogenesis differentiation at early stage, but failed to induce the ALP-expression pre-osteoblast to mature osteoblast. Also, we analyzed the effect of 1000 nM genistein on the adipocyte differentiation of healthy-MSCs. Compared to the control group, no significant changes were shown in the Oil-Red-O staining and the mRNA expression level of master adipogenesis regulators (Pparg and Cebpa) and adipocyte-specific genes (Fabp4 and Lpl) in the genistein group (Supplementary Fig. S1e, f).

We next examined the effect of genistein on the autophagy activity of healthy-MSCs. No significant changes of protein expression of LC3-II, P62, active-β-catenin and APC were observed by 1–1000 nM genistein treatment for 48 h (Fig. 8f). As 1000 nM genistein could enhance ALP activity, we specifically examined the effect of 1000 nM genistein on autophagy flux of healthy-MSCs. Healthy-MSCs transfected with mRFP-GFP-LC3 construct showed a lot of red puncta (autolysosome) in the cells (Fig. 8g). When the healthy-MSCs were treated by Baf-A1, we observed markedly increased yellow puncta and the protein level of LC3-II and P62 (Fig. 8g, h). These results demonstrated that the healthy-MSCs maintained a high level of basal autophagic activity. However, compared to the control group, no significant changes in the mRFP-GFP-LC3 fluorescence microscopy and the protein

expression of LC3-II and P62 were shown in the 1000 nM genistein group.

We further used murine C3H10T1/2 mesenchymal stem cells to test this hypothesis. Like healthy-MSCs, no significant increase in ALP staining or alizarin red staining were observed in C3H10T1/2 cells by the 1–1000 nM genistein treatments (Supplementary Fig. S1g). The immunoblotting assay also demonstrated no significant changes in APC or active-β-catenin protein level in C3H10T1/2 cells undergoing osteogenic differentiation or genistein treatment (Supplementary Fig. S1h, i). Strikingly, the protein expressions of LC3-II and P62 in C3H10T1/2 cells treated by osteogenic medium indicated that the autophagy was blocked at 24 h and 48 h (Supplementary Fig. S1h, i). Administration of genistein at 1000 and 10 nM for 24 h and 48 h were not able to activate autophagy in C3H10T1/2 cells (Supplementary Fig. S1h, i).

Collectively, the above results demonstrated that the osteogenesis promoting effect of genistein on healthy-MSCs was independent of autophagy.

DISCUSSION

In this study, we showed that autophagy activated by genistein promoted osteoblastic differentiation of OVX-MSCs through positively regulating Wnt signaling. Notably, we demonstrated that APC functioned as a key cellular integration factor to mediate autophagy-stimulated Wnt/β-catenin signaling activation.

The canonical Wnt/β-catenin signaling pathway plays an important role in osteoblast differentiation of MSCs through its main effector, β-catenin [16]. The relationship between autophagy and Wnt/β-catenin signaling is somewhat controversial. Moreover, the exact mechanisms of how autophagy regulates Wnt/β-catenin signaling are poorly understood. Some researchers found that the enhanced autophagy can directly degrade β-catenin in multiple colorectal carcinoma cell lines [38, 39], others reported that autophagy indirectly downregulated β-catenin by promoting Dvl2 degradation in human HEK293T cells, murine embryonic fibroblasts and non-small cell lung cancer cells [40–42]. Also, in the myoblasts differentiation and thymic epithelial cells development, the aberrant activated autophagy could degrade Dvl2 to inhibit Wnt/β-catenin signaling, resulting in hypogenesis and atrophy [43, 44]. Other studies, on the contrary, have shown positive relationship between autophagy and Wnt/β-catenin signaling. In preadipocytes, TP53INP2 activates Wnt/β-catenin signaling through autophagy-dependent sequestration of GSK3β into late endosomes [45]. In human non-small lung adenocarcinoma A549 cells, inhibiting autophagy by chloroquine attenuates Wnt/β-catenin signaling by downregulating the protein level of p-GSK3β [46]. Notch signaling plays an important role in osteoblast differentiation, and its activation impairs the osteoblast differentiation and inhibits the Wnt/β-catenin signaling. Recently, Yoshimori et al. [47] demonstrated that genetic upregulation of autophagy by deleting RUBCN (a negative regulator of autophagy) in osteoblasts promoted osteogenic differentiation via autophagic degradation of NOTCH intracellular domain (NICD) and down-regulation of Notch signaling pathway. Liu et al. [48] found that the tuberous sclerosis complex 1 (TSC1)-deficient BMSCs exhibited inhibited autophagy and increased Notch1 protein level, which led to the decreased β-catenin protein level and impaired osteoblast differentiation. It can be concluded that autophagy activated by different stimuli in different cell types may degrade different cellular proteins and thus have opposite effects on Wnt/β-catenin signaling.

Our data showed that genistein promoted autophagosome clearance of APC protein in OVX-MSCs, and thus inhibited the destruction of β-catenin. In line with the result of our study, Park et al. [49] also found that TMEM9 activated Wnt/β-catenin signaling by lysosomal degradation of APC, and treatment of Baf-A1 inhibited the down-regulation of APC protein level. The co-localization of APC and LC3 was also observed in neurons [50], and inhibition of autophagy by FSIP1 knockdown enhanced the APC protein level [51]. Since the upstream mediators of autophagy are important in targeting cellular protein for degradation, we found that genistein activated autophagy through TFEB rather than mTOR. Similarly, Deng et al. [52] reported that negative pressure induced osteogenic differentiation of MSCs via autophagy activation, and the activation of autophagy was mediated by AMPK-ULK1 axis rather than mTOR. We also found that resveratrol, a TFEB agonist which activates TFEB through AMPK [53], was able to activate autophagy, upregulate active-β-catenin level and downregulate APC level in OVX-MSCs. Quercetin was reported to promote TFEB nuclear translocation and enhance its transcriptional activity via mTOR inhibition in cultured RPE cells [54]. However, we did not observe significant changes in autophagy and active-β-catenin level in quercetin-treated OVX-MSCs. Intriguingly, although the APC and P62 protein level were decreased at 36 h and 48 h of genistein treatment, the APC level was restored while the P62 was downergulated at 72 h. Since β-catenin represses P62 expression at transcriptional level [38], it is likely the reduced P62 protein expression at 72 h is due to P62 mRNA downregulation rather than autophagic degradation.

In this study, the protein levels of total β-catenin, active-β-catenin and LC3-II were significantly elevated during 48 h of genistein treatment, followed by a decline at 72 h of genistein treatment. These data demonstrated a complex, time-dependent modulation of Wnt/β-catenin signaling and autophagy during osteoblast differentiation of OVX-MSCs. The temporal relationship between osteoblastic differentiation and autophagy in MSCs has been uncovered: during osteoblastic differentiation the autophagic activity is enhanced in the initial 2 days and declined thereafter [24], and persistent autophagy activation results in inhibited osteogenesis [55]. The Wnt/β-catenin signaling could inhibit autophagy by downregulating the P62 level [56] or through GSK-3β/TSC2/mTORC1 pathway [57]. Thus, it can be speculated that Wnt/β-catenin signaling participated in a homeostatic feedback loop to limit prolonged autophagic activation.

In order to investigate the similarities/differences in the responses of genistein-treated healthy-MSCs and OVX-MSCs, we performed experiments on the healthy-MSCs isolated from 6-month-old female rats. Our results are consistent with those reported in the literature also describing that genistein could upregulate the BMP2 expression, but failed to stimulate the maturation and mineralization of pre-osteoblast [58]. Consistent with other studies [5, 59], we also found that the healthy-MSCs maintained a high level of basal autophagy. Genistein treatment could not further enhance the autophagic activity in healthy-MSCs, which may be accounted for the weak osteogenesis promotion effect of genistein on healthy-MSCs.

The impaired osteoblastic differentiation in OVX-MSCs is reported partially due to a deficiency in general autophagy [60], a failure to degrade specific proteins and protein aggregates. Our study indicates that early interventions aimed at restoring autophagic flux may be beneficial to rebalance the dysregulated osteoblast-adipocyte lineage differentiation in OVX-MSCs. Despite remarkable progress in drug development was achieved, most of the current therapies for treating postmenopausal osteoporosis are anti-resorptive drugs. The insight into the molecular mechanisms of autophagy governing the differentiation of OVX-MSC can facilitate developing new therapies to treat postmenopausal osteoporosis.

CONCLUSIONS

From the results of the present study, we demonstrated that genistein promotes osteoblast differentiation of OVX-MSCs through autophagy-Wnt/β-catenin pathway. Notably, autophagy

upregulates active-β-catenin protein level by promoting autophagic degradation of APC. Instead of mTOR, genistein activates autophagy mainly through TFEB in OVX-MSCs. We hope that the molecular mechanisms of autophagy governing the differentiation of OVX-MSC can facilitate developing new therapies to treat postmenopausal osteoporosis.

ACKNOWLEDGEMENTS

This study was supported by the National Natural Science Foundation of China (grant number, 32000976 and 82071134).

AUTHOR CONTRIBUTIONS

JG designed the experiments and wrote the manuscript. JG, YJY, JYL, and MYL performed most of the experiments. KX prepared the bone specimens and performed the histology. SMX generated the OVX rat model. SYW contributed to analysis and interpretation of data. CY supervised the study, and revised manuscript critically for important intellectual content. All authors have read and approved the manuscript.

ADDITIONAL INFORMATION

Supplementary information The online version contains supplementary material available at https://doi.org/10.1038/s41401-023-01066-x.

Competing interests: The authors declare no competing interests.

REFERENCES

1. Nollet M, Santucci-Darmanin S, Breuil V, Al-Sahlanee R, Cros C, Topi M, et al. Autophagy in osteoblasts is involved in mineralization and bone homeostasis. Autophagy. 2014;10:1965–77.
2. Li HX, Li DH, Ma ZM, Qian Z, Kang XM, Jin XX, et al. Defective autophagy in osteoblasts induces endoplasmic reticulum stress and causes remarkable bone loss. Autophagy. 2018;14:1726–41.
3. Yang C, Tao HQ, Zhang HF, Xia Y, Bai JX, Ge GR, et al. TET2 regulates osteoclastogenesis by modulating autophagy in OVX-induced bone loss. Autophagy. 2022;18:2817–29.
4. Li X, Xu JK, Dai BY, Wang XL, Guo QY, Qin L. Targeting autophagy in osteoporosis: From pathophysiology to potential therapy. Ageing Res Rev. 2020;62:101098.
5. Qi M, Zhang LQ, Ma Y, Shuai Y, Li LY, Luo KF, et al. Autophagy maintains the function of bone marrow mesenchymal stem cells to prevent estrogen deficiency-induced osteoporosis. Theranostics. 2017;7:4498–516.
6. Atteritano M, Mazzaferro S, Frisina A, Cannata ML, Bitto A, D'Anna R, et al. Genistein effects on quantitative ultrasound parameters and bone mineral density in osteopenic postmenopausal women. Osteoporos Int. 2009;20:1947–54.
7. Arcoraci V, Atteritano M, Squadrito F, D'Anna R, Marini H, Santoro D, et al. Anti-osteoporotic activity of genistein aglycone in postmenopausal women: evidence from a post-hoc analysis of a multicenter randomized controlled trial. Nutrients. 2017;9:179.
8. Hertrampf T, Gruca MJ, Seibel J, Laudenbach U, Fritzemeier KH, Diel P. The bone-protective effect of the phytoestrogen genistein is mediated via ER alpha-dependent mechanisms and strongly enhanced by physical activity. Bone. 2007;40:1529–35.
9. Bitto A, Burnett BP, Polito F, Marini H, Levy RM, Armbruster MA, et al. Effects of genistein aglycone in osteoporotic, ovariectomized rats: a comparison with alendronate, raloxifene and oestradiol. Br J Pharmacol. 2008;155:896–905.
10. Dai J, Li YL, Zhou HH, Chen J, Chen MH, Xiao ZS. Genistein promotion of osteogenic differentiation through BMP2/SMAD5/RUNX2 signaling. Int J Biol Sci. 2013;9:1089–98.
11. Liao QC, Xiao ZS, Qin YF, Zhou HH. Genistein stimulates osteoblastic differentiation via p38 MAPK-Cbfa1 pathway in bone marrow culture. Acta Pharmacol Sin. 2007;28:1597–602.
12. Pan W, Quarles LD, Song LH, Yu YH, Jiao C, Tang HB, et al. Genistein stimulates the osteoblastic differentiation via NO/cGMP in bone marrow culture. J Cell Biochem. 2005;94:307–16.
13. Zhou S, Turgeman G, Harris SE, Leitman DC, Komm BS, Bodine PV, et al. Estrogens activate bone morphogenetic protein-2 gene transcription in mouse mesenchymal stem cells. Mol Endocrinol. 2003;17:56–66.
14. Nabavi SF, Sureda A, Dehpour AR, Shirooie S, Silva AS, Devi KP, et al. Regulation of autophagy by polyphenols: Paving the road for treatment of neurodegeneration. Biotechnol Adv. 2018;36:1768–78.
15. Hasima H, Ozpolat B. Regulation of autophagy by polyphenolic compounds as a potential therapeutic strategy for cancer. Cell Death Dis. 2014;5:e1509.
16. Song L, Liu M, Ono N, Bringhurst FR, Kronenberg HM, Guo J. Loss of wnt/β-catenin signaling causes cell fate shift of preosteoblasts from osteoblasts to adipocytes. J Bone Min Res. 2012;27:2344–58.
17. Ranes M, Zaleska M, Sakalas S, Knight R, Guettler S. Reconstitution of the destruction complex defines roles of AXIN polymers and APC in β-catenin capture, phosphorylation, and ubiquitylation. Mol Cell. 2021;81:3246–61.e3211
18. Wang T, Bai JX, Lu M, Huang CL, Geng DC, Chen G, et al. Engineering immunomodulatory and osteoinductive implant surfaces via mussel adhesion-mediated ion coordination and molecular clicking. Nat Commun. 2022;13:160.
19. Xi G, Wai C, Rosen CJ, Clemmons DR. A peptide containing the receptor binding site of insulin-like growth factor binding protein-2 enhances bone mass in ovariectomized rats. Bone Res. 2018;6:23.
20. Soleimani M, Nadri S. A protocol for isolation and culture of mesenchymal stem cells from mouse bone marrow. Nat Protoc. 2009;4:102–6.
21. Bai JX, Ge GR, Wang Q, Li WM, Zheng K, Xu YZ, et al. Engineering stem cell recruitment and osteoinduction via bioadhesive molecular mimics to improve osteoporotic bone-implant integration. Research (Wash DC). 2022;2022:9823784.
22. Deng P, Yuan Q, Cheng YD, Li J, Liu ZQ, Liu Y, et al. Loss of KDM4B exacerbates bone-fat imbalance and mesenchymal stromal cell exhaustion in skeletal aging. Cell Stem Cell. 2021;28:1057–73.e1057.
23. Klionsky DJ, Abdelmohsen K, Abe A, Abedin MJ, Abeliovich H, Acevedo Arozena A, et al. Guidelines for the use and interpretation of assays for monitoring autophagy (3rd edition). Autophagy. 2016;12:1–222.
24. Pantovic A, Krstic A, Janjetovic K, Kocic J, Harhaji-Trajkovic L, Bugarski D, et al. Coordinated time-dependent modulation of AMPK/Akt/mTOR signaling and autophagy controls osteogenic differentiation of human mesenchymal stem cells. Bone. 2013;52:524–31.
25. Nuschke A, Rodrigues M, Stolz DB, Chu CT, Griffith L, Wells A. Human mesenchymal stem cells/multipotent stromal cells consume accumulated autophagosomes early in differentiation. Stem Cell Res Ther. 2014;5:140.
26. Eskelinen EL, Schmidt CK, Neu S, Willenborg M, Fuertes G, Salvador N, et al. Disturbed cholesterol traffic but normal proteolytic function in LAMP-1/LAMP-2 double-deficient fibroblasts. Mol Biol Cell. 2004;15:3132–45.
27. van der Horst G, van der Werf SM, Farih-Sips H, van Bezooijen RL, Löwik CW, Karperien M. Downregulation of Wnt signaling by increased expression of Dickkopf-1 and -2 is a prerequisite for late-stage osteoblast differentiation of KS483 cells. J Bone Min Res. 2005;20:1867–77.
28. Nusse R, Clevers H. Wnt/β-Catenin signaling, disease, and emerging therapeutic modalities. Cell. 2017;169:985–99.
29. Pohl C, Dikic I. Cellular quality control by the ubiquitin-proteasome system and autophagy. Science. 2019;366:818–22.
30. Casares-Crespo L, Calatayud-Baselga I, García-Corzo L, Mira H. On the Role of basal autophagy in adult neural stem cells and neurogenesis. Front Cell Neurosci. 2018;12:339.
31. Jacomin AC, Samavedam S, Promponas V, Nezis IP. iLIR database: A web resource for LIR motif-containing proteins in eukaryotes. Autophagy. 2016;12:1945–53.
32. Zhou YN, Wu YQ, Ma WD, Jiang XQ, Takemra A, Uemura M, et al. The effect of quercetin delivery system on osteogenesis and angiogenesis under osteoporotic conditions. J Mater Chem. B 2017;5:612–25.
33. Li J, Xin ZX, Cai MJ. The role of resveratrol in bone marrow-derived mesenchymal stem cells from patients with osteoporosis. J Cell Biochem. 2019;120:16634–42.
34. Louvet L, Leterme D, Delplace S, Miellot F, Marchandise P, Gauthier V, et al. Sirtuin 1 deficiency decreases bone mass and increases bone marrow adiposity in a mouse model of chronic energy deficiency. Bone. 2020;136:115361.
35. Nakamura S, Shigeyama S, Minami S, Shima T, Akayama S, Matsuda T, et al. LC3 lipidation is essential for TFEB activation during the lysosomal damage response to kidney injury. Nat Cell Biol. 2020;22:1252–63.
36. Chau MN, El Touny LH, Jagadeesh S, Banerjee PP. Physiologically achievable concentrations of genistein enhance telomerase activity in prostate cancer cells via the activation of STAT3. Carcinogenesis. 2007;28:2282–90.
37. Zhang LY, Xue HG, Chen JY, Chai W, Ni M. Genistein induces adipogenic differentiation in human bone marrow mesenchymal stem cells and suppresses their osteogenic potential by upregulating PPARγ. Exp Ther Med. 2016;11:1853–8.
38. Petherick KJ, Williams AC, Lane JD, Ordóñez-Morán P, Huelsken J, Collard TJ, et al. Autolysosomal β-catenin degradation regulates Wnt-autophagy-p62 crosstalk. Embo J. 2013;32:1903–16.
39. Wu H, Lu XX, Wang JR, Yang TY, Li XM, He XS, et al. TRAF6 inhibits colorectal cancer metastasis through regulating selective autophagic CTNNB1/β-catenin degradation and is targeted for GSK3B/GSK3β-mediated phosphorylation and degradation. Autophagy. 2019;15:1506–22.
40. Gao C, Cao WP, Bao L, Zuo W, Xie GM, Cai TT, et al. Autophagy negatively regulates Wnt signalling by promoting Dishevelled degradation. Nat Cell Biol. 2010;12:781–90.

41. Cheng MZ, Xue H, Cao WP, Li WX, Chen H, Liu BF, et al. Receptor for activated c kinase 1 (RACK1) promotes dishevelled protein degradation via autophagy and antagonizes wnt signaling. J Biol Chem. 2016;291:12871–9.
42. Luo XM, Ye SJ, Jiang QQ, Gong Y, Yuan Y, Hu XT, et al. Wnt inhibitory factor-1-mediated autophagy inhibits Wnt/β-catenin signaling by downregulating dishevelled-2 expression in non-small cell lung cancer cells. Int J Oncol. 2018;53:904–14.
43. Liang ZF, Zhang LJ, Su HT, Luan R, Na N, Sun LN, et al. MTOR signaling is essential for the development of thymic epithelial cells and the induction of central immune tolerance. Autophagy 2018;14:505–17.
44. Zhang K, Zhang YY, Gu LJ, Lan MM, Liu CC, Wang M, et al. Islr regulates canonical Wnt signaling-mediated skeletal muscle regeneration by stabilizing Dishevelled-2 and preventing autophagy. Nat Commun. 2018;9:5129.
45. Romero M, Sabaté-Pérez A, Francis VA, Castrillón-Rodriguez I, Díaz-Ramos A, Sánchez-Feutrie M, et al. TP53INP2 regulates adiposity by activating β-catenin through autophagy-dependent sequestration of GSK3β. Nat Cell Biol. 2018;20:443–54.
46. Datta S, Choudhury D, Das A, Mukherjee DD, Dasgupta M, Bandopadhyay S, et al. Autophagy inhibition with chloroquine reverts paclitaxel resistance and attenuates metastatic potential in human nonsmall lung adenocarcinoma A549 cells via ROS mediated modulation of β-catenin pathway. Apoptosis. 2019;24:414–33.
47. Yoshida G, Kawabata T, Takamatsu H, Saita S, Nakamura S, Nishikawa K, et al. Degradation of the NOTCH intracellular domain by elevated autophagy in osteoblasts promotes osteoblast differentiation and alleviates osteoporosis. Autophagy. 2022;18:2323–32.
48. Choi HK, Yuan H, Fang F, Wei X, Liu L, Li Q, et al. Tsc1 regulates the balance between osteoblast and adipocyte differentiation through autophagy/notch1/β-catenin cascade. J Bone Min Res. 2018;33:2021–34.
49. Jung YS, Jun S, Kim MJ, Lee SH, Suh HN, Lien EM, et al. TMEM9 promotes intestinal tumorigenesis through vacuolar-ATPase-activated Wnt/β-catenin signalling. Nat Cell Biol. 2018;20:1421–33.
50. Sarkar C, Zhao Z, Aungst S, Sabirzhanov B, Faden AI, Lipinski MM. Impaired autophagy flux is associated with neuronal cell death after traumatic brain injury. Autophagy. 2014;10:2208–22.
51. Liu CG, Sun LS, Yang J, Liu T, Yang YL, Kim SM, et al. FSIP1 regulates autophagy in breast cancer. Proc Natl Acad Sci USA. 2018;115:13075–80.
52. Zhang S, Xie YL, Yan FF, Zhang YF, Yang ZQ, Chen Z, et al. Negative pressure wound therapy improves bone regeneration by promoting osteogenic differentiation via the AMPK-ULK1-autophagy axis. Autophagy. 2022;18:2229–45.
53. Chen MY, Dai YS, Liu SY, Fan YX, Ding ZX, Li D. TFEB biology and agonists at a glance. Cells. 2021;10:333.
54. Huang Y, Chen Y, Shaw AM, Goldfine H, Tian JQ, Cai JY. Enhancing TFEB-mediated cellular degradation pathways by the mTORC1 inhibitor quercetin. Oxid Med Cell Longev. 2018;2018:5073420.
55. Schaub T, Gürgen D, Maus D, Lange C, Tarabykin V, Dragun D, et al. mTORC1 and mTORC2 differentially regulate cell fate programs to coordinate osteoblastic differentiation in mesenchymal stromal cells. Sci Rep. 2019;9:20071.
56. Nàger M, Sallán MC, Visa A, Pushparaj C, Santacana M, Macià A, et al. Inhibition of WNT-CTNNB1 signaling upregulates SQSTM1 and sensitizes glioblastoma cells to autophagy blockers. Autophagy. 2018;14:619–36.
57. Shimobayashi M, Hall MN. Making new contacts: the mTOR network in metabolism and signalling crosstalk. Nat Rev Mol Cell Biol. 2014;15:155–62.
58. Heim M, Frank O, Kampmann G, Sochocky N, Pennimpede T, Fuchs P, et al. The phytoestrogen genistein enhances osteogenesis and represses adipogenic differentiation of human primary bone marrow stromal cells. Endocrinology. 2004;145:848–59.
59. Oliver L, Hue E, Priault M, Vallette FM. Basal autophagy decreased during the differentiation of human adult mesenchymal stem cells. Stem Cells Dev. 2012;21:2779–88.
60. Florencio-Silva R, Sasso GRS, Sasso-Cerri E, Simões MJ, Cerri PS. Effects of estrogen status in osteocyte autophagy and its relation to osteocyte viability in alveolar process of ovariectomized rats. Biomed Pharmacother. 2018;98:406–15.